

NASA Contractor Report 3802

NASA-CR-3802 19840021819

Magnetic Suspension and Balance System Study

R. W. Boom, Y. M. Eyssa, G. E. McIntosh,
and M. K. Abdelsalam

CONTRACT NAS1-17428
JULY 1984

LIBRARY COPY

JUL 10 1984

LANGLEY RESEARCH CENTER
LIBRARY
11111

NASA



NASA Contractor Report 3802

Magnetic Suspension and Balance System Study

R. W. Boom, Y. M. Eyssa, G. E. McIntosh,
and M. K. Abdelsalam

Madison Magnetics, Inc.
Madison, Wisconsin

Prepared for
Langley Research Center
under Contract NAS1-17428



National Aeronautics
and Space Administration

Scientific and Technical
Information Branch

1984

March 1, 1984

FOREWORD

This report is a design and cost study for a Magnetic Suspension and Balance System suitable for an 8 ft. x 8 ft test section at Mach 0.9 with 0.1% control forces at 10 Hz for an F16 model airplane.

R. W. Boom, Y. M. Eyssa, G. E. McIntosh and M. K. Abdelsalam are the major contributors to the study.

TABLE OF CONTENTS

	<u>Page</u>
Foreword.....	iii
Table of Contents.....	iv
List of Figures.....	vii
List of Tables.....	ix
References.....	xi
I. Introduction.....	I-1
I.1 Background.....	I-1
I.2 Summary	I-2
II. MSBS Requirements.....	II-1
II.1 Objective.....	II-1
II.1.1 Model Visual Access.....	II-1
II.1.2 Operational Duty Cycle.....	II-1
II.1.3 Static Forces and Moments.....	II-3
II.1.4 Model Angular Displacement Range.....	II-6
II.1.5 System Availability.....	II-6
II.2 Tunnel Constraints.....	II-7
III. System Configuration.....	III-1
III.1 Model Core.....	III-2
III.1.1 Model Core Magnetic Analysis.....	III-2
III.2 Z and Y Gradient Coils.....	III-3
III.3 Drag Coils (X Coils).....	III-6
III.4 Roll Coils (R Coils).....	III-6

III.4.1	Permanent Magnet Materials.....	III-9
III.4.2.	Wing Configuration.....	III-11
III.4.3	Roll Coil Configuration.....	III-14
III.5	Cross Coupling.....	III-17
III.5.1	Drag Coils (X Coils).....	III-19
III.5.2	Z Gradient Coils.....	III-20
III.5.3	Y Gradient Coils.....	III-21
III.5.4	Field Requirement.....	III-21
IV.	Magnet Design	IV-1
IV.1	Magnet System Requirement.....	IV-1
IV.1.1	Coil Shapes.....	IV-1
IV.1.2	Coil Peak Fields.....	IV-1
IV.1.3	Coil Terminal Voltages.....	IV-3
IV.1.4	Coil Structural Design.....	IV-3
IV.1.6	Magnet Control Requirement.....	IV-5
IV.2	Conductor.....	IV-5
IV.2.1	Conductor Cooling and Stability.....	IV-7
IV.3	Magnet System Concept.....	IV-8
IV.3.1	System Analysis.....	IV-8
IV.3.2	Model Core Solenoid.....	IV-10
IV.3.3	X, Y, Z and R Coils.....	IV-17
V.	Structural and Thermal Design.....	V-1
V.1	Introduction.....	V-1
V.2	Materials.....	V-2
V.3	Forces and Torques.....	V-9

V.4	Structural Design.....	V-9
V.5	Electrical Isolation.....	V-14
V.6	Weight Summary.....	V-17
V.7	Cryostat Support.....	V-17
V.8	Cryostat Heat Leak.....	V-20
VI.	Cryogenic System.....	VI-1
VI.1	Introduction.....	VI-1
VI.2	Magnet Power Leads.....	VI-1
VI.3	Operating Losses.....	VI-3
VI.4	Component Design and Sizing.....	VI-3
VI.5	Component Discussion.....	VI-7
VI.6	Component Cost Estimates.....	VI-12
VI.7	Cooldown Analysis.....	VI-14
VI.8	Operating Plan.....	VI-14
VII.	Scaling Relations.....	VII-1
VII.1	Force and Torque Scaling.....	VII-1
VII.2	Model Core Scaling.....	VII-1
VII.3	Ampere Meter Scaling.....	VII-4
VIII.	Cost Estimate.....	VIII-1
IX.	Conclusion.....	IX-1
X.	Recommendations for Future Studies.....	X-1

LIST OF FIGURES

		<u>Page</u>
Figure I.1	Magnet System	I-4
Figure III.1	Z or Y Gradient Coils	III-5
Figure III.2	Drag Coil and Model Coil Location	III-7
Figure III.3	$F(\Delta, \ell)$ and Δ vs. ℓ for optimization of location and size of drag coils for given values of F_x , L, and R.	III-8
Figure III.4	F16 Wing	III-12
Figure III.5	Wing cross-sectional area at any chord length C showing stainless steel support, skin, and permanent magnet material	III-13
Figure III.6	Roll Field Distribution	III-15
Figure III.7	Torque Requirement Across Wing	III-16
Figure III.8	Magnet System	III-18
Figure IV.1	Cryostable 11 kA AC Cable	IV-6
Figure IV.2	Core Magnet Cryostat	IV-11
Figure V.1	Preliminary Arrangement	V-3
Figure V.2	MSBS Cryostat Views	V-4
Figure V.3	Cryostat Cut Away Isometric	V-5
Figure V.4	MSBS General Assembly	V-6
Figure V.5	Egg Crate Design Schematic	V-12
Figure V.6	Bottom Plate Seal & Electric Insulator	V-15
Figure V.7	Egg Crate Seal & Electrical Liner Insulator	V-16

Figure	V.8	Leg Assembly Concept	V-19
Figure	VI.1	MSBS Cryogenic Schematic	VI-9
Figure	VI.2	Co-Axial Transfer Line	VI-11

LIST OF TABLES

			<u>Page</u>
Table	I-1	MSBS Design Comparison	I-5
Table	I-2	Cryogen and Power Usage	I-7
Table	II-1	MSBS Requirements 8' x 8' Test Section	II-2
Table	II-2	Field Requirements in Tesla at Pole Tips for Maximum Angles of Pitch (α), Yaw (β), and Roll (ϕ)	II-5
Table	II-3	Time Constants for Field Diffusion through Dewar Walls	II-8
Table	III-1	Comparison of Model Core Magnetic Pole Strengths	III-4
Table	III-3	Properties of Some Permanent Magnet Materials	III-10
Table	IV-1	Maximum Fields in Coils	IV-2
Table	IV-2	Voltage and Power Requirements	IV-4
Table	IV-3	Inductance Matrix in Milli Henries	IV-9
Table	IV-4	Model Coil Parameters	IV-12
Table	IV-5	X Drag Coil Parameters	IV-13
Table	IV-6	Y Gradient Coil Parameters	IV-14
Table	IV-7	Z Gradient Coil Parameters	IV-15
Table	IV-8	R Coil Parameters	IV-16
Table	IV-9	Ampere Meters and Stored Energy	IV-17
Table	IV-10	Coil Weights, kg	IV-18
Table	IV-11	Coil AC Losses at 10 Hz	IV-20
Table	IV-12	Eddy Current Losses in the External Structure	IV-21

Table	V-1	Coil Forces and Torques	V-10
Table	V-2	Eddy Current Forces Between Structure and Coils at Full Load	V-11
Table	V-3	Estimated Weights of Magnets and Structure	V-18
Table	V-4	Static Heat Leak and Cryogen Consumption	V-20
Table	VI-1	Predicted Lead Losses	VI-2
Table	VI-2	Magnet Cryostat Operating Losses	VI-4
Table	VI-3	Cryogenic Components for Continuous Operation	VI-6
Table	VI-4	Cryogenic Components for Five-Day Week Operation	VI-7
Table	VI-5	Cryogenic System Cost Estimates	VI-13
Table	VII-1	Scaling of Magnetic Field and Field Gradient at the Model	VII-3
Table	VII-2	Ampere Meter Requirement for the 8' x 8' Wind Tunnel	VII-4
Table	VII-3	Total Ampere Meters as a Function of L/8	VII-5
Table	VIII-1	MSBS Cost Estimate (Case 1 - Alternate G)	VIII-3

REFERENCES

- (1) H. L. Bloom et al.: Design Concepts and Cost Studies for Magnetic Suspension and Balance Systems. NASA CR-165917, July 1982.
- (2) C. P. Britcher: Some Aspects of Wind Tunnel Magnetic Suspension Systems with Special Application at Large Physical Scales. NASA CR-172154, September 1983.
- (3) S. H. Kim, S. T. Wang and M. Lieberg: Advances in Cryogenic Engineering, vol. 25, Plenum Press, N.Y. 1980, pp. 90 - 97.
- (4) R. J. Loyd et al.: Conceptual Design and Cost of a Superconducting Magnetic Energy Storage Plant. Electric Power Research Institute, EPRI-EM-3457, April 1984.
- (5) S. J. Sackett: EFFI: A Code for Calculating the Electromagnetic Field, Force, and Inductance in Coil Systems of Arbitrary Geometry. Lawrence Livermore Laboratory, Livermore, California. UCRL-52402, March 1978.
- (6) C. P. Britcher, M. J. Goodyer, R. G. Scurlock and Y. Y. Wu: A Flying Super-Conducting Magnet and Cryostat for Magnetic Suspension of Wind-Tunnel Models. Cryogenics, vol. 24, no. 4, April 1984, pp. 185 - 189.

I. INTRODUCTION

I.1 BACKGROUND

Magnetic suspension and balance systems (MSBS) have been used to support models for aerodynamic tests in wind tunnel facilities for over 25 years. The primary advantage of a MSBS is the complete elimination of support interference effects which can result from the use of mechanical model support systems such as stings and struts. The air flow over a test model can be affected both by the physical proximity of a mechanical support and by the alterations to the actual model shape which are often required to accommodate mechanical supports. A secondary advantage of a MSBS is the ease and flexibility with which the test model may be positioned in the wind tunnel air stream in both the rotational and translational degrees of freedom.

The useful size of the wind tunnel test sections of the MSBS constructed, to date, have ranged in diameter from about 10 centimeters to 33 centimeters. As part of its research relative to the development of advanced wind tunnel concepts and aerodynamic testing techniques, the NASA Langley Research Center has been sponsoring studies to investigate the application of MSBS to wind tunnels having a test section large enough to accommodate the detailed three-dimensional models required for configuration research and aerospace vehicle development. The results of a study in 1981 (reference 1) made the consideration of a large 2.4 meters by 2.4 meters (8 feet by 8 feet) size test section for a transonic wind tunnel with superconducting electromagnets appear to be practical and feasible. However, before the size and force capacity of such a technically desirable large MSBS can be selected, additional

information is needed to allow performance and size trade-offs to be made. The purpose of this study is to make a detailed evaluation, using advanced concepts where possible, of one specific option, Alternate G, developed for a large MSBS in reference 1.

I.2 SUMMARY

The cost estimate for this MSBS design is \$29,939,000 which is to be compared to \$88,448,000 for Case 1-Alternate G, the reference starting design for an 8 ft. x 8 ft. wind tunnel.

Cost reductions are achieved by the following design choices,

- Superconductive persistent solenoid in the suspended airplane model which increases the model magnetic moment by 73.6% with attendant X, Y and Z coil reductions.
- Elimination of two magnetization coils accounting for about 10% of magnet costs.
- Permanent magnet wings resulting in a 20% improvement in achieved wing magnetic pole strength.
- New roll coil design providing 0.3 tesla at wing tips.
- Roll torque specifications are 100% achieved vs. 50% for magnetized soft iron wings.
- Compact magnet design in one common dewar with internal reinforcement resulting in minimum structure and a low static heat leak of 45 W at 4.2 K.
- Stainless steel internal cold intermagnet structure with attendant AC eddy current losses is accommodated without fiberglass epoxy dewars.

- Magnet location and size optimization.
- 44% reduction in conductor ampere meters.
- 47% reduction in stored energy and structure.
- Only 560 liters/hour helium liquefier is needed even with stainless steel structure.
- Maximum coil OD is 15% less at 8.10 m (drag coil).

The procedure followed in the MSBS design is to concentrate exclusively on Case 1-Alternate G specifications. Each component is optimized for maximum efficiency. The system configuration is given in Fig. I.1. Y, Z, and R roll magnets are mounted on rectangular walls closely surrounding the tunnel. The race track R coils are especially efficient. All interactive forces are taken internally without external heat leak. The X drag coils are a minimum diameter because of the compact nature of the system.

The magnets are all designed for use in 4.2 K one atmosphere liquid helium with the established 11 kA cryostable⁽³⁾ Argonne National Laboratory AC conductor. There is more than adequate space for interleaved 304 stainless steel structural banding between turns.

In chapter II the Specifications for Case 1-Alternate G are listed as to forces and torques on the model. The AC losses occur in the magnets and cold structure at the control frequency of 10 Hz for continuous disturbance of 0.1% I in any coil. Full load corresponds to 0.1% I_{\max} in all coils simultaneously at 10 Hz; quarter load is for 0.1% ($I_{\max}/4$) at 10 Hz.

Chapter III describes the Configurations for all magnet coils, the model superconducting core solenoid and the permanent magnet wings. The magnets are optimized as to dimensions and locations to produce the required forces and torques. Cross-coupling is accounted for in all cases. As an example of

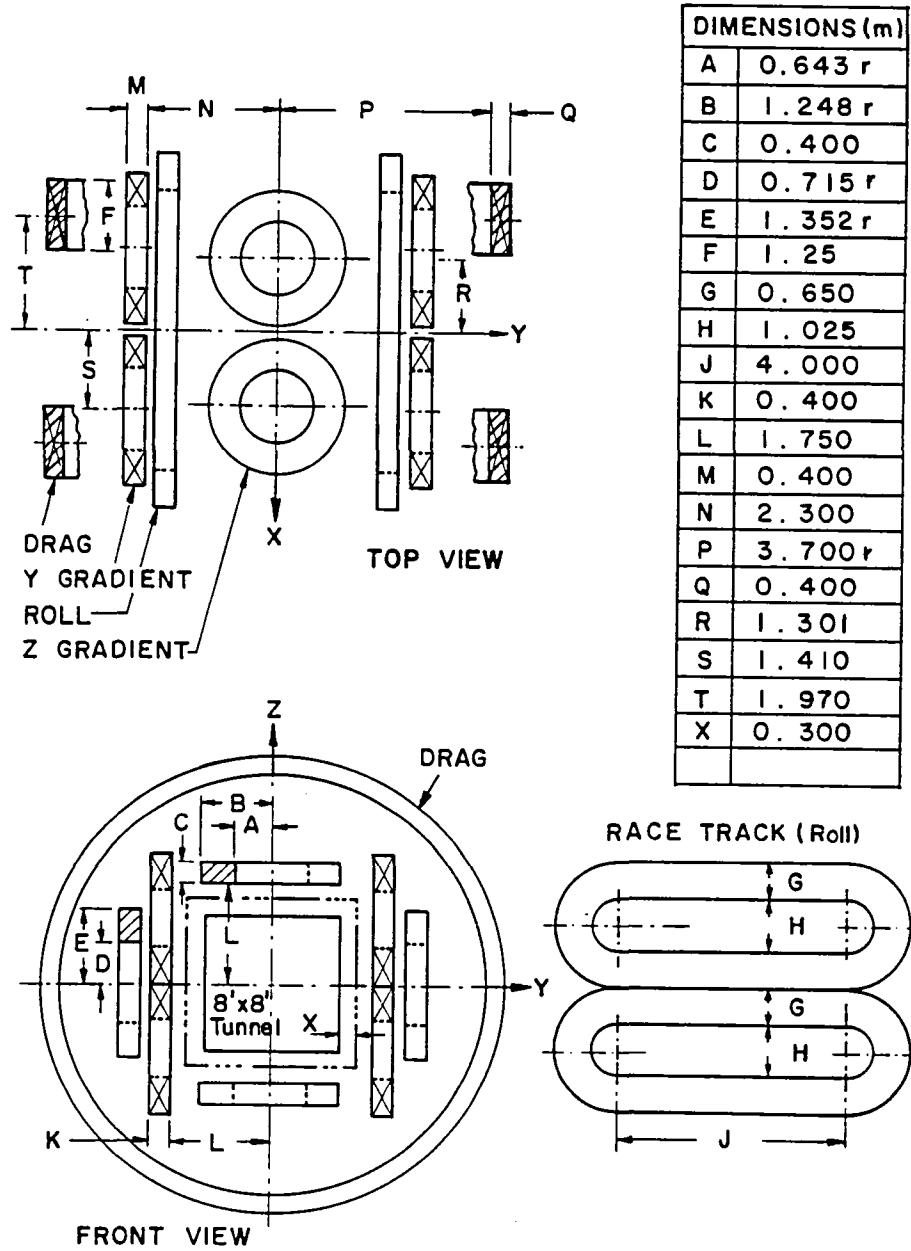


Figure I-1. Magnet System

TABLE I-1
MSBS DESIGN COMPARISON
MADISON MAGNETICS, INC. DESIGN

Madison Magnetics Design	Z	Y	Roll	Drag	Total
Ampere-Meters (MAm)	86	100	207	362	755
Energy Stored (MJ)	50	60	140	656	906
Maximum Field (tesla)	5.8	6.3	6.1	4.4	

GENERAL ELECTRIC CO. DESIGN

General Electric Design	Z	Y	Roll	Drag + Magnetize	Total
Ampere-Meters (MAm)	374	51(?)	233	508 + 180	1346
Energy Stored (MJ)	592	56(?)	248	758 + 52	1706
Maximum Field (tesla)	7.7	4	4	4	

cross-coupling consider the Y coils which are responsible for Yaw torques. The Y coils must have extra turns to counteract cross-coupled Yaw torques on the model from all other coils.

Chapter IV covers the Magnet System Design as to detailed sizes, forces and torques. Table I-1 is a comparison of the Madison Magnetics, Inc. (MMI) design with the previous GE design. The MMI ampere meters are 56% of GE and the MMI stored energy is 53% of GE. The Y coil for GE is surprisingly small compared to the other GE coils. MMI improvements stem from the compact, single dewar design, from a new race track roll coil system and from a superconducting model core magnet.

The conductor design is explained as regards the cable construction and stability in 4.2 K liquid helium pool cooling. AC losses in the coils during dynamic 10 Hz control are 405 watts at full load and 189 watts at 1/4 load. There are 11 power supplies with total power of about 100 MW to meet the 10 Hz requirement.

Chapter V covers the design of a massive cold Structure assembly to which all of the magnets are attached and all magnets, except for the two drag coils, are cooled in a single large liquid helium container. The mutual magnet forces are reacted by the large cold rectangular mounting structure. The wind tunnel is surrounded by an "egg crate" load-bearing wall which reacts atmospheric pressure on one side and helium pressure on the other side. The major structure is a rectangle reinforced with spaced webs. Overall weight is about 367,600 Kg.

Eddy current losses in the steel structure are tolerable for all coils except the X drag coils. To reduce X coil eddy current losses the cold

structure at 4.2 K is slotted bottom center in the $y = 0$ plane the full length of the structure. Therefore there is no closed circuit of structure paralleling the X coil turns. Even the thin 0.51 mm S.S. liner to hold helium is slotted. The AC losses for the structure comprise about 70% of the 4.2 K helium requirement at full load.

Chapter VI covers Cryogenics requirements and the design of the cryogenic system flow diagram. The key features are a 560 liter/h helium liquefier, 47,500 liter helium storage dewar, 39,644 m³ gas storage facility, 0.543 m³/s helium recovery compressor, LN₂ heat exchangers and 354 m³ helium gas bag. Cooldown is approximately eight days. The system can operate at 100% load for two hours and 25% load for eight hours continuously without exhausting the liquid helium supply. Recharging during down times can keep the liquid storage dewar half full which provides sufficient capacity to run 1.5 standard days without a liquefier.

The daily operational requirements are given in Table I-2 for power and for cryogenics.

TABLE I-2
CRYOGEN AND POWER USAGE

	Full Load 2 h	Quarter Load 8 h	Stand-by 14 h
Liquid Helium	3120 ℓ/h	590 ℓ/h	175 ℓ/h
Liquid Nitrogen	13 ℓ/h	13 ℓ/h	13 ℓ/h
Power Supplies	100 MW	6.3 MW	0

Chapter VII describes Scaling to different size wind tunnels from the present 8' x 8' cross-section. Forces scale as $(L/8)^2$ and torques as $(L/8)^3$ due to the model length being proportional to tunnel length L. For models with magnetized iron or permanent magnet cores and wings the external field at the pole tips remains the same. The field gradient scales as $8/L$. For superconducting model cores the external field at model pole tips varies smoothly from $1.65 B_0$ at $L = 4$ ft to $0.75 B_0$ at $L = 16$ ft where $B = B_0$ at 8 ft.

The use of superconducting cores for the airplane model scales favorably for larger tunnels and is already better than magnetized iron by 73% in an 8 ft tunnel. The break-even tunnel size between superconducting cores and magnetized iron cores is about a 4 ft tunnel. A 12 ft tunnel would require about 2.25 times as large a magnet set for magnetized iron as for a superconducting model core solenoid.

Chapter VIII lists the Cost Estimates for the MSBS system following the outline and maintaining the rates used in NASA CR 165917. Major savings result from reduced materials and labor for a small, compact and simple magnet system. The 11 kA cable and magnet winding cost is based on known ANL costs.

The \$29,939,000 cost for an 8 ft. by 8 ft. Mach 0.9 wind tunnel represents industrial costs on the same basis as in NASA CR 165917.

Chapter IX Conclusion is a brief description of the major features of this MSBS study.

Chapter X lists Recommendations for further studies.

II. MSBS REQUIREMENTS

The MSBS specifications and requirements are listed in Table II-1. The forces on a suspended airplane model in the wind tunnel are equal to the product of magnetic pole strengths in the model multiplied by the applied magnetic field. The core and wing dimensions determine the maximum volume available for the on-board magnetic poles and moments. The magnetic fields necessary to provide the required forces and moments in the angular range listed are provided by an external set of magnet coils. The dynamic force requirements at 10 Hz are needed for feedback control to maintain model positioning during operation.

II.1 OBJECTIVE

The object of this study is to design a superconductive magnet system optimized for economic performance encompassing the listed requirements.

II.1.1 Model Visual Access

The optimized configuration chosen by Madison Magnetics does not allow visual observation and access to the model. Observation must be via indirect optical or electronic systems. In any case, the presence of high magnetic fields would limit human observation. All equipment located close to the MSBS coils, including viewing equipment, must be capable of operation in high magnetic fields. A television display could replace visual observation.

II.1.2 Operational Duty Cycle

The operational duty cycle per day is two hours at full load, eight hours at quarter load and 14 hours standby. Full load is defined as the 10 Hz control of 0.1% I at maximum current in all coils. This provides 10 Hz

TABLE II-1. MSBS REQUIREMENTS
8' x 8' TEST SECTION

A. Static Force Requirements	
Lift	9790 N
Side	1380 N
Drag	4180 N
B. Static Moment Capability	
Pitch	420 Nm
Yaw	140 Nm
Roll	140 Nm
C. Angular Displacement Range	
Angle of Attack (α)	$\pm 30^\circ$
Angle of Sideslip (β)	$\pm 10^\circ$
Angle of Roll (ϕ)	$\pm 20^\circ$
D. Core Dimensions	
Length	75 cm
Diameter	12.7 cm
E. Wing Dimensions	(see Fig. III.4)
F. Dynamic Force Requirements, $\pm 0.1\%$ at 10 Hz	
Lift	± 9.79 N
Side	± 1.38 N
Drag	± 4.18 N

control at maximum angles of pitch, yaw and roll with sufficient magnetic forces to balance these wind forces. The operational duty cycle thus sets the requirements for helium usage and electrical power, both of which are maximum at full load.

An operational duty cycle might be five days of the above schedule and two days at zero load which provides time to liquefy extra helium for a five-day week. In this case a smaller liquefier and larger helium storage is required for a net saving of \$100,000 out of a total capital cost of about \$2,600,000.

II.1.3 Static Forces and Moments

The requirements for static forces and moments are listed in Table II-1. If the model is replaced by a magnet of a length L and a pole strength Q , then the force in the i^{th} direction for $+ B_i$ at the north pole and $- B_i$ at the south pole (typical of MSBS fields) is

$$F_i = 2Q B_i \quad , \quad (\text{II.1})$$

where F_i = force in the i^{th} direction, N

Q = model magnet pole strength, Am

B_i = magnetic field in the i^{th} direction at the core tips

i = x, y, or z.

The magnetic field at the poles of the core, B_i , is the field due to all coils in the i^{th} direction at any position of pitch and/or yaw.

The pitch and yaw torques are

$$T_p = Q L \delta B_z \cos \alpha \quad , \quad (II.2)$$

and
$$T_y = Q L \delta B_y \cos \beta \quad , \quad (II.3)$$

where δB_z and δB_y are the difference in B_z and B_y at the model tips. δB_z appears in Eq. II.2 because the F_z forces at each end of the pole tip are in the same direction and result in a torque only if one $F_{z1} = QB_{z1}$ is larger than the other $F_{z2} = QB_{z2}$, or $\delta B = |B_{z1} - B_{z2}| > 0$. The pitch and yaw angles are α and β .

The roll torque at any roll angle ϕ is

$$T_r \approx 2 q b B_z(\phi=0) \{ \cos^2 \phi - \sin^2 \phi \} \quad (II.4)$$

where q is an equivalent magnetic pole strength of the permanent magnets in the wing tips and $2b$ is the equivalent span. Details of these definitions are provided in Chapter III. $B_z(\phi=0)$ is the z component of the magnetic field at the tip of the wing for $\phi=0$.

The static force and torque requirements listed in Table II-1 are the values required at the maximum angles of $\pm 30^\circ$ in pitch, $\pm 10^\circ$ in yaw and $\pm 20^\circ$ in roll. The forces and torques from Eqs. II.1, 2, 3 and 4 determine the required field components at maximum angles of pitch, yaw and roll. A model superconducting coil of pole strength $Q = 3.75 \times 10^4$ Am and length of 70 cm is used to determine the field components in Table II-2. The wing is of permanent magnet material, with a span $2b = 82$ cm, see Section III.4.2.

TABLE II-2
 FIELD REQUIREMENTS IN TESLA AT POLE TIPS FOR MAXIMUM ANGLES
 OF PITCH (α), YAW (β), AND ROLL (ϕ)

	LIFT	LATERAL	DRAG	ROLL
Field component	B_z^*	B_y^*	B_x	B_z
Field location	$\alpha = 30^\circ$ $\beta = 10^\circ$	$\alpha = 30^\circ$ $\beta = 10^\circ$	$\alpha = 30^\circ$ $\beta = 10^\circ$	$\phi = 20^\circ$
Field required to produce force	0.1305	0.0184	0.0557	-
Field required to produce torque	0.0184	0.0054	-	0.3
Total field	0.149	0.024	0.0557	0.3
Margin for control	2%	2%	2%	2%
Total Field required	0.152 T	0.0243 T	0.057 T	0.306 T

*Fields are in negative direction of z and y axis when α and β are positive and vice versa.

II.1.4 Model Angular Displacement Range

The MSBS coils are designed to provide the required forces and torques within the specified angular displacements of $\pm 30^{\circ}$ in pitch, $\pm 10^{\circ}$ in yaw, and $\pm 20^{\circ}$ in roll. Extra ampere turns are provided to account for control and for cross coupling between coils. The roll torques can be easily satisfied with permanent wing magnets with an average magnetization of 0.70 to 0.75 tesla and an applied field at the wing tips of about 0.30 tesla.

II.1.5 System Availability

The system availability should be as high as possible. The anticipated availability is 91.6% based on a two year assessment of the Wisconsin Energy Storage Solenoid System.⁽⁴⁾ In that case,

$$\begin{aligned} \text{OA} &= (1 - \text{POR}) (1 - \text{UOR}) \\ &= (1 - .04) (1 - .046) \\ &= 91.6\% \end{aligned}$$

where

OA = Operating Availability

POR = Planned Outage Rate

UOR = Unplanned Outage Rate.

The values of POR and UOR are somewhat subjective since they are based on 30 years of bubble chamber magnet experience in which there were no outages. The values POR = 0.04 and UOR = 0.046 are the author's opinion that there might be a single three month outage in a 40 year period, for an unknown reason. In addition, no reason could be given for planned outages although a value is assumed.

In the utility industry where 70% availability is normal a rating of 92% is considered unprecedented. The basic reason for the high availability is the combined operating experience of bubble chamber superconducting solenoids. In about 30 years of operation at ANL, FERMI and CERN there has been no unplanned outage. The ANL solenoid went normal once without damage due to inadvertent high rate current ramping with the solenoid dewar only half full of helium.

The MSBS proposed conductor and magnet manufacturing scheme is almost identical with that used by ANL. The cable conductor to be used has repeatedly withstood continuous 11 tesla/sec sawtooth ramps in test coils while remaining superconducting. In contrast the MSBS solenoids will never be subjected to more than 0.24 tesla/sec.

Failure modes such as loss of cooling and loss of power are allowed for. To quote reference (4): "No specific technical requirements were identified for establishing a non-zero planned outage rate. This is because there are no moving parts in the coil, corrosion of components inside of the vacuum enclosure is unlikely, and because all systems are redundant and can be maintained without shutting down the plant."

II.2 Tunnel Constraints

The "stay-out" zone of one foot on all sides requires that the MSBS be mounted outside a 10' x 10' region.

The 10 Hz requirement for dynamic field control requires that a 10 Hz field variation must be transmitted through intervening walls. In NASA CR 165917⁽¹⁾ this problem was approached by estimating the time constants for

TABLE II-3
 TIME CONSTANTS FOR FIELD DIFFUSION
 THROUGH DEWAR WALLS
 8 x 8 Foot Test Section

	MMI Design	NASA CR 165917 ⁽¹⁾	
Wall Thickness	2 mm	25.4 mm	50.8 mm
Stainless Steel $\rho = 50 \times 10^{-6} \Omega\text{cm}$ at low temperature	0.00315 sec	0.04 sec	0.08 sec
Characteristic time at 10 Hz for field change		$\tau \sim \frac{1}{f} = 0.1 \text{ sec}$	

field diffusion through the intervening wall. The intervening wall was modeled as an infinite cylinder between the magnet system and the airplane model. Table II-3 reproduces the field diffusion chart with an additional entry for the presently planned MMI low temperature stainless steel wall thickness.

If the test section has a time constant comparable to $\tau = 0.1$ sec then severe field wave form distortion results. Note that the MMI wall thickness of 2 mm has a time constant about 1/30 of the field driving time constant and would produce negligible distortion.

A similar conclusion can be drawn from skin depth δ which measures depth of penetration of an incident wave. The skin depth is the distance within a conductor at a point at which the amplitude of the field vector is equal to $1/e = 0.3679$ of its value at the surface.

$$\begin{aligned}\delta &= (2 \rho / \mu \omega)^{1/2} \\ &= 36 f^{-1/2} \text{ cm for S.S. at low temperature} \\ &= 11.4 \text{ cm at 10 Hz.}\end{aligned}$$

A wall 2 mm thick is almost transparent.

Separately mounted coils require heavy cold structural steel walls in each dewar through which field changes must diffuse. Such steel walls in the 2.54 cm thickness range are unacceptable as to field distortion and lead to selecting non-metallic (epoxy) structures.

The MMI design mounts all magnets inside heavy steel structure with only 2 mm cold stainless steel walls between the coils and the model. Such favorable design is the direct consequence of mounting all coils in one common dewar.

III. SYSTEM CONFIGURATION

The magnet system configuration for the 8' by 8' tunnel provides the magnetic fields to produce the static forces and torques needed to control the model in the six degrees of freedom. The system configuration is summarized as follows.

-- A 70 cm long potted persistent superconducting solenoidal coil, 11.5 cm O.D., and 6.1 tesla is the model core. A superconducting coil produces higher magnetic moments and pole strengths than a magnetized iron core or a permanent magnet core.

-- The model wings contain permanent magnets that occupy 85 percent of the wing volume. The rest of the wing volume is high strength stainless steel.

-- Z and Y gradient coils are symmetric arrays of four solenoid magnets each. They are bipolar coils to control and manipulate the model. The conductor for all coil systems is the 11-kA low-loss cryostable conductor.⁽³⁾

-- The drag coils to counterbalance wind drag forces are large diameter solenoids.

-- The roll coils are four race-track coils optimized for minimum ampere meters.

The magnets are optimized as to dimension and location subject to the required forces, torques, maximum magnetic fields in the windings and gross current density of 1500 A/cm^2 in the coils.

III.1 MODEL CORE

The model core size is 75 cm long and 125 cm² in cross-sectional area. The model core can be either a permanent magnet with an average remanent magnetism of 1 tesla, or soft iron magnetized by a pair of external coils at 2 tesla saturation magnetization, or a superconducting coil in a helium dewar. A superconducting coil could produce fields up to 7 tesla. We compare the magnetic pole strength in the three cases and show that the superconducting coil is a better choice than either a soft iron core or a permanent magnet core for the model size in a 8' x 8' tunnel.

III.1.1 Model Core Magnetic Analysis

Assume the following superconducting coil nomenclature:

R = outer radius of the model dewar

b = outer radius of the model coil

a = inner radius of the model coil

$\delta = R - b = 6$ mm (dewar + insulation thickness, see Chapter VI)

L = model coil length = 70 cm

J = gross current density = 30,000 A/cm²,

and the maximum magnetic field at the midplane of a long solenoid is

$$B_m = \mu_0 J(b-a), \quad (\text{III.1})$$

The magnetic pole strength is

$$Q = \pi J(b^3 - a^3)/3 \quad . \quad (\text{III.2})$$

Using Eqs. (III.1) and (III.2), Q is

$$Q = \pi J \left\{ (R-\delta)^3 - \left(R-\delta - \frac{B_m}{\mu_0 J} \right)^3 \right\} \quad . \quad (\text{III.3})$$

For a magnetized saturated iron core Q becomes

$$Q = \frac{MA}{\mu_0} \quad , \quad (\text{III.4})$$

where A is equal to 0.0125 m^2 , $M = 2 \text{ tesla}$ and $\mu_0 = 4\pi 10^{-7}$.

As seen in Table III-1, a superconducting core is superior compared to magnetized soft iron core for $R > 5 \text{ cm}$. Within the 125 cm^2 cross-sectional area of the model a superconducting coil can produce a pole strength $Q = 3.7 \times 10^4 \text{ Am}$, which is about 70% higher than Q for magnetized soft iron. The superconducting core results in smaller Z, Y and X coils.

III.2 Z AND Y GRADIENT COILS

Based on previous studies^(1,2) a configuration of four bipolar coils is chosen to provide forces and torques in the z and y directions. Their functions are identical except for the direction and magnitude of forces and torques produced. Consider a set of four coils, either Y or Z, as shown in Figure III.1. The design task is to find the dimensions S, R_1 , R_2 , and t subject to the constraints:

- required forces and torques,
- maximum self field in windings, and
- gross current density $\cong 1500 \text{ amp/cm}^2$.

TABLE III-1
 COMPARISON OF MODEL CORE MAGNETIC POLE STRENGTHS Q_m IN Am
 FOR 6.1 TESLA SUPERCONDUCTING COIL,
 FOR MAGNETIZED IRON AT 2 TESLA,
 AND FOR A PERMANENT MAGNET AT
 1 TESLA AS FUNCTIONS OF MODEL
 OUTSIDE RADIUS (R)

R (inches)	R (cm)	6.1 T Coil ($Q_m \times 10^4$)	Magnetized Iron* ($Q_m \times 10^4$)	Permanent Magnet* ($Q_m \times 10^4$)
6"	15.24	29.2	12.4	6.2
5.5"	13.97	25.0	10.5	5.23
5"	12.7	19.47	8.64	4.32
4.5"	11.43	15.34	7.0	3.5
4"	10.16	11.71	5.53	2.76
3.5"	8.89	8.57	4.76	2.38
3"	7.62	5.92	3.11	1.56
2.5"	6.35	3.75	2.16	1.08
2"	5.08	2.01	1.38	0.69
1.5"	3.81	0.912	0.77	0.39

*Pole strength is multiplied by 75/70 to account for the difference in model length from the superconducting coil.

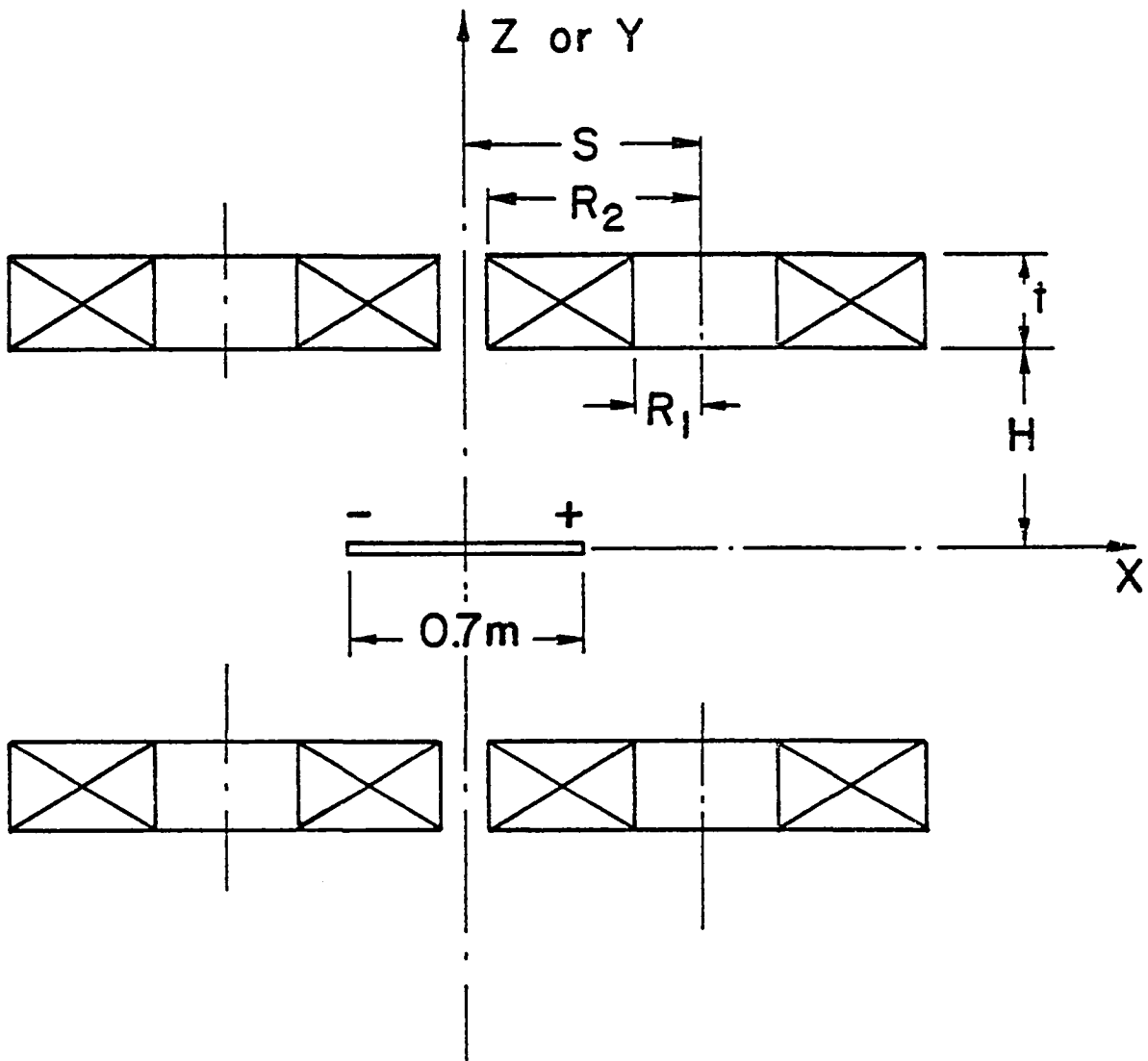


Figure III.1. Z or Y Gradient Coils

The required dimensions, ampere meters and stored energy are found through a series of iterations. This optimization provides the coil dimensions and location for minimum ampere meters and stored energy.

III.3 DRAG COILS (X COILS)

The drag coils provide a field gradient at the model coil which produces an axial force to resist the drag force of the wind. Because of the low drag force compared to the lift force, the drag coils enclose the Z gradient coils. Once the radius of the two drag coils is known, their optimized location can be easily found, Figure III.2. The drag force per coil is

$$F_x = \frac{\mu_0 NIQ}{2R} \left\{ \frac{1}{(1+\Delta)^2} \right\}^{3/2} - \frac{1}{(1+(\Delta+l)^2)^{3/2}} \quad , \quad \text{N/coil} \quad \text{(III.5)}$$

$$\text{where } \Delta = \frac{S}{R} \quad , \quad l = \frac{L}{R} \quad ,$$

$$\text{and } F_x = \frac{\mu_0 NIQ}{2R} F(\Delta, l) \quad . \quad \text{N/coil}$$

To find the minimum value of ampere turns NI per required Force F_x , the function $F(\Delta, l)$ is optimized. Figure III.3 is a sketch of the optimized values for $F(\Delta, l)$ and Δ as functions of l .

III.4 ROLL COILS (R COILS)

The roll coils provide a field on the magnetic wings to produce roll torque on the model. The magnetization of the wing can be either permanent magnetization (SPM) or induced magnetization (SIM).

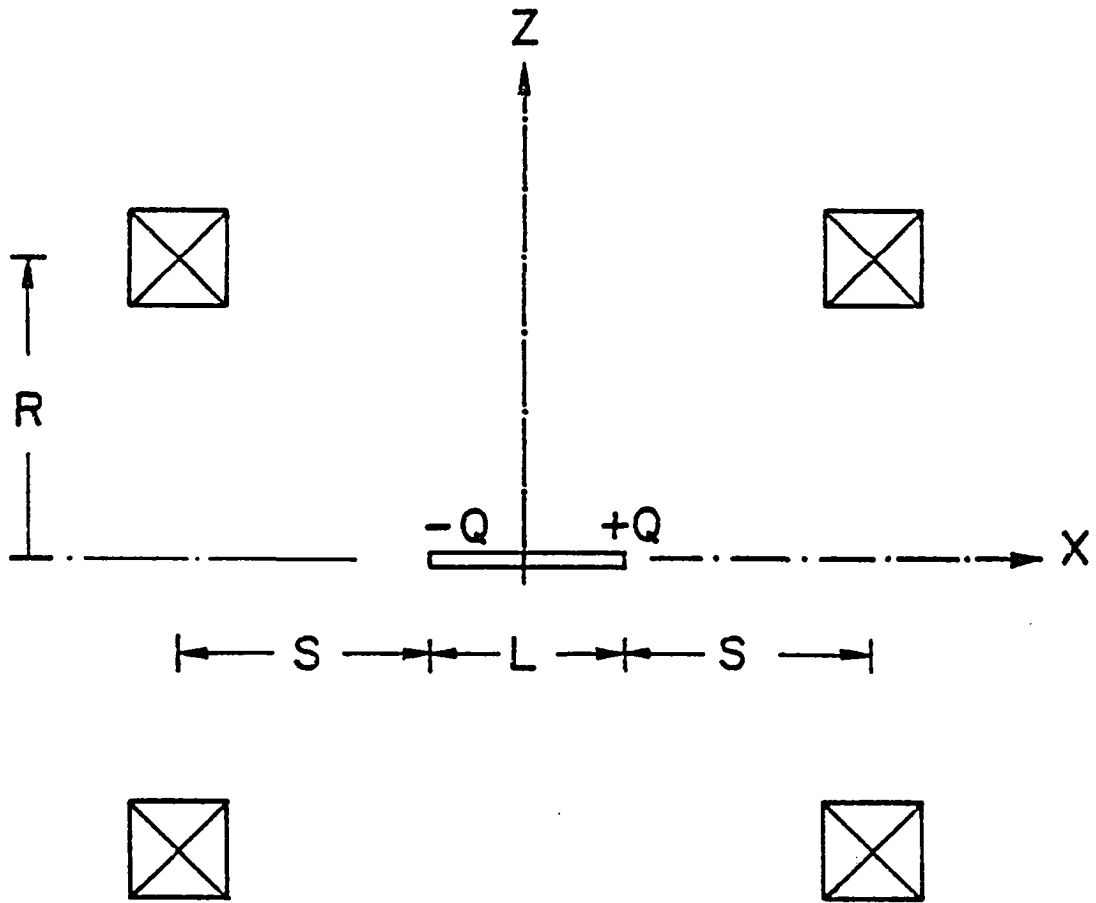


Figure III.2. Drag Coil and Model Coil Locations

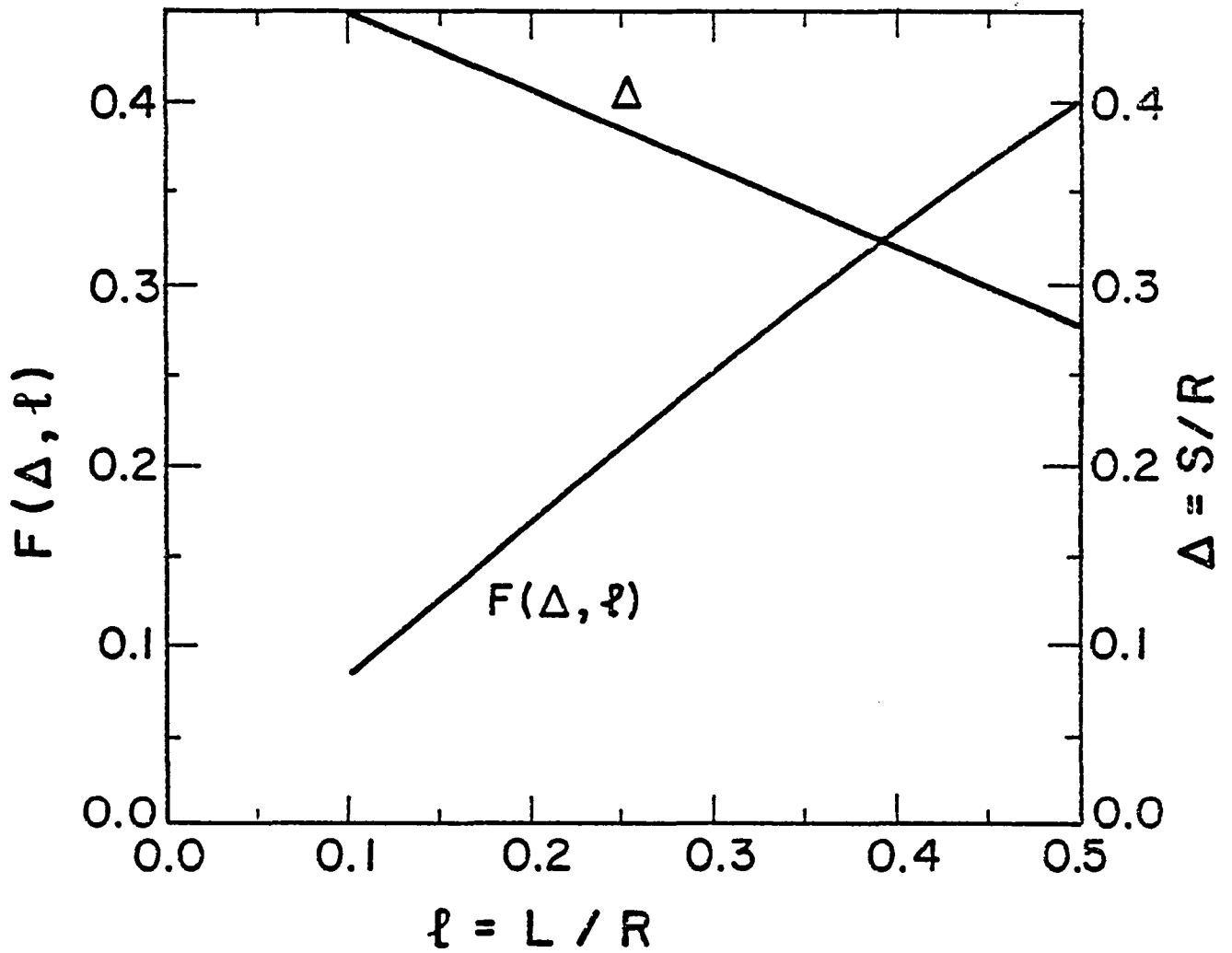


Figure III.3. $F(\Delta, \ell)$ and Δ vs. ℓ for optimization of location and size of drag coils for given values of F_x , L , and R .

The analysis of SIM has been recognized as complicated. A previous study⁽¹⁾ used greatly simplified approximate analyses to design the 8 roll coils. A more representative analysis, as in reference 2, is applicable to this configuration but would require further study which is beyond the present scope of work. We use the SPM permanent magnet wings and race track roll coils which allow accurate field calculation. The wings are of high coercive force permanent magnet materials with remanent magnetization on the order of 0.9 tesla such as Re Co.⁽²⁾

III.4.1 Permanent Magnet Materials

The conventional parameters to characterize any permanent magnet material are B_r , the remanent magnetism, and H_c , the coercive force. Another useful parameter H_k (2) is the demagnetizing field at which the permanent magnet material loses 10% of its remanent magnetism. The field H_k is applied opposite to B_r to demagnetize the permanent magnet material. Applying H_r at right angles to B_r should result in insignificant reduction in the values of B_r , which is the case for the roll coils. Table III-3 lists B_r , H_c and H_k for some strong permanent magnet alloys.

Based on the roll torque requirements the externally applied field on the wing will range from 0.0 at the center to 0.30 tesla at the tip. The magnetic material in the wing should be the Sm Co₅ "RECOMA 20" or graded from materials 2, 5, and 4 in Table III-3 depending on the field distribution at the wing. Because the field at the wing is normal to B_r it may be possible to use values higher than H_k without much change in the value of B_r . Because of the poor mechanical properties of the strong permanent magnet materials listed in Table

TABLE III-3
 PROPERTIES OF SOME PERMANENT MAGNET MATERIALS

Material	B_r (T)	H_c (T)	H_k (T)
1. Sintered (3) SM Co ₅	0.85	1.5	1.13
2. SM Co ₅ based (4) "Recoma 20"	0.90	1.5	1.25
3. "Commercial" (5) SM Co ₅	0.84	1.0	0.613
4. Alnico 5 DG (6)	1.33	0.068	0.04
5. Alnico g (6)	1.04	0.16	0.10

(3)
 (4)
 (5)
 (6) — In Reference (2) see listed references 25, 32 and 33.

III-3, the wing should contain some other strong non-magnetic alloy such as stainless steel. It is found from mechanical design that 15% of the cross-section should be stainless steel. Accordingly, the magnetic material is 85% of the wing volume for an average magnetization of 0.7 to 0.75 tesla for an ungraded wing using alloy No. 2 in Table III-3. An average magnetization of 0.8 tesla may be obtained by grading with other alloys.

III.4.2 Wing Configuration

The wing configuration is that of the F16 fighter model. The arrangement of the wing plan form is shown in Figs. III.4 and III.5. Using the non-dimensionalized airfoil coordinates provided by NASA, the cross-sectional area A at any chord of length C is

$$A = 0.02625 C^2 \quad \text{cm}^2 .$$

At the tip where $C = 9.8$ cm, A is 2.52 cm^2 while at the fuselage where $C = 43.18$ cm, A is 48.9 cm^2 . Actually the wing starts at $y = 6$ cm which is the outer radius of the model core and extends to $y = 41$ cm at the tip. The cross-sectional area A at any distance y is

$$A(y) = 48.4 - 1.8453 y - 0.0173952 y^2 \quad \text{cm}^2. \quad (\text{III.6})$$

Taking M as the average magnetization in the y direction, it is easy to show that the net torque is

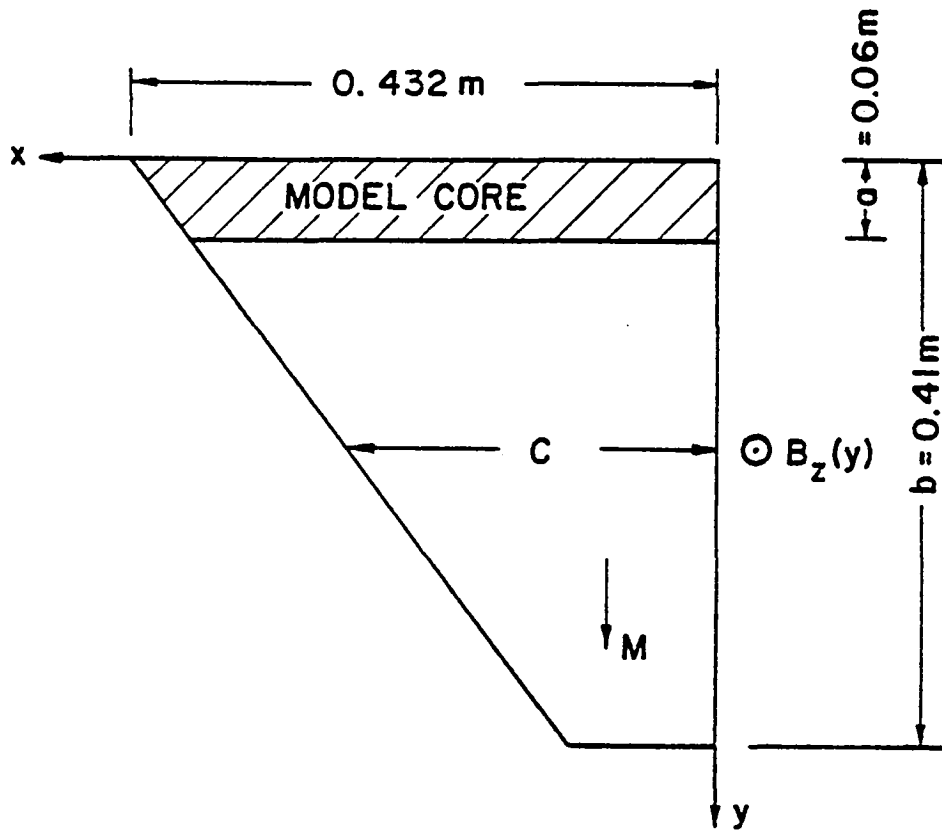


Figure III.4. F16 Wing

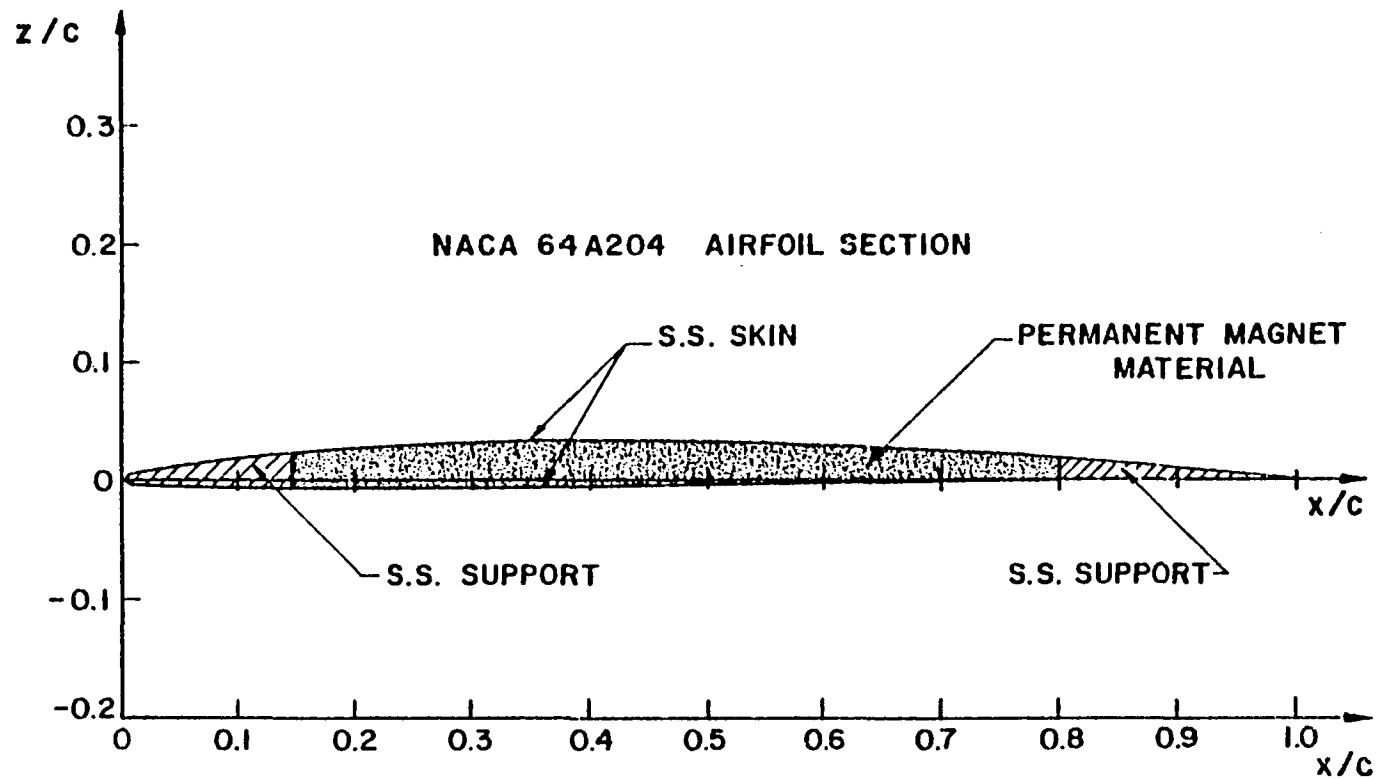


Figure III.5. Wing cross-sectional area at any chord length C showing stainless steel support, skin, and permanent magnet material.

$$T_r = \frac{2}{\mu_0} \{ bMA(b)B_z(b) - aMA(a)B_z(a) + M \int_a^b B_z(y)y dA_y \} \quad (III.7)$$

where $a = 0.06$ m, $b = 0.41$ m, and $B_z(y)$ is

$$B_z(y) = B_z(b) \frac{y}{b} .$$

B_z and M are in tesla while distances are in meters and T_r is in Nm.

From the above equations the magnetic field $B_z(b)$ at the tip of the wing is

$$B_z(b) \approx 4\pi 10^{-4} \frac{T_r}{M} ,$$

where T_r is the torque at zero roll angle ϕ . To produce a torque of 141 Nm at $\pm 20^\circ$,

$$T_r = 141 / (\cos^2 20^\circ - \sin^2 20^\circ) = 184 \text{ Nm.}$$

For an average magnetization of 0.6 tesla $B_z(b) = 0.385$ tesla, and for $M = 0.7$ tesla, $B_z(b) = 0.300$ tesla.

III.4.3 Roll Coil Configuration

The R coils produce a z component of magnetic field of 0.30 tesla at the wing tips to produce roll angles $\pm 20^\circ$. The field should be an odd function of y to produce zero field at the fuselage (the model core) for minimum cross

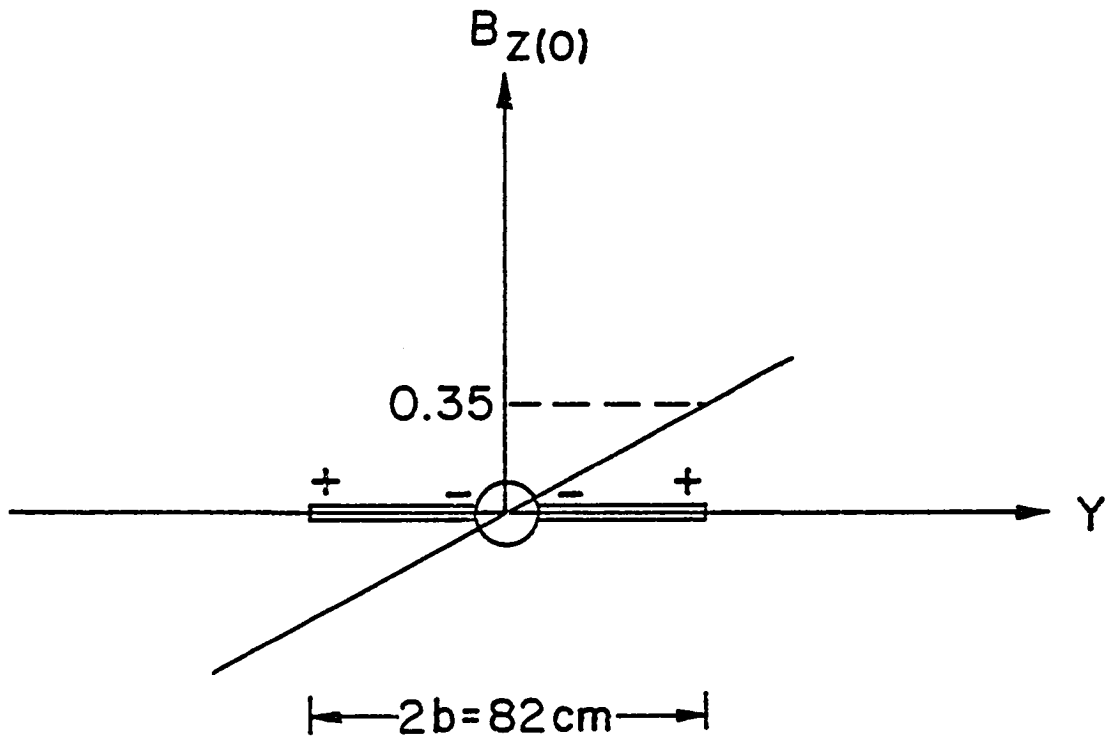


Figure III.6. Roll Field Distribution

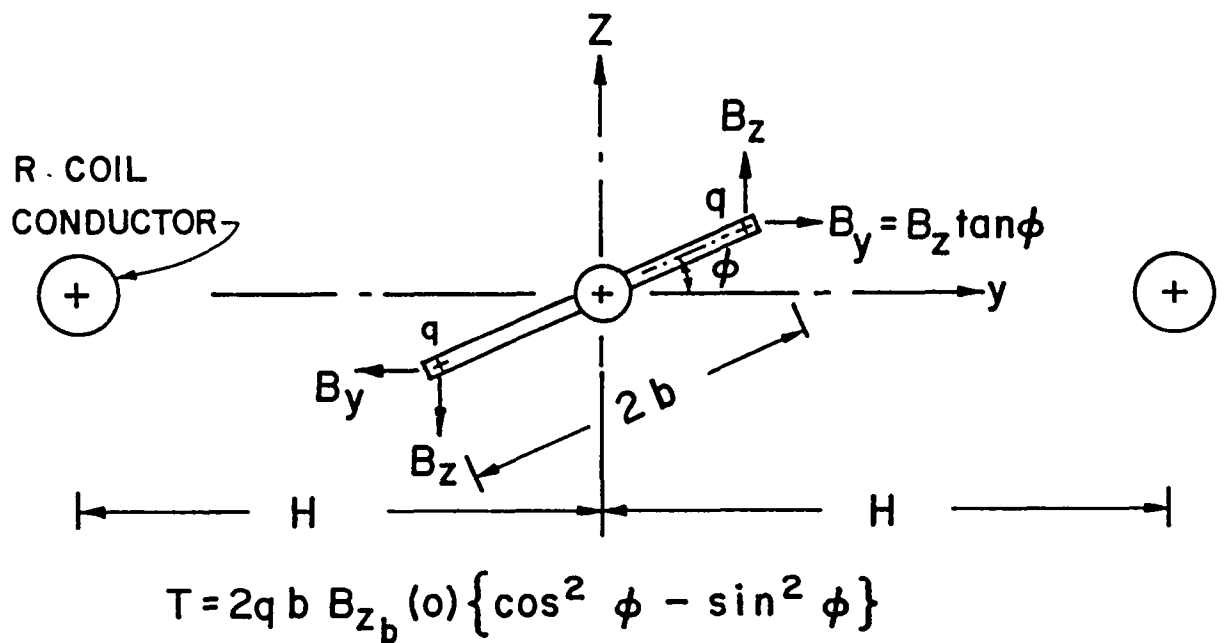


Figure III.7. Torque Requirement Across Wing

coupling interaction. When the model pitches or yaws cross coupling components will exist. Details about cross coupling are discussed in III.5. Figure III.6 shows the roll field and Figure III.7 the torque requirement across the wing span. The field configuration is produced by two straight wires in the x direction placed on the $Z = 0$ plane at $y = \pm H$ and carrying a current in the same direction as shown in Figure III.7. For minimum current requirements, the distance H is as small as possible. The present 8 foot x 8 foot tunnel with a one foot stay out zone and 25.4 cm needed for dewar insulation and structure becomes 3.56 m x 3.56 m at the magnet edges. Thus $H \cong 1.78$ m + half the winding thickness. The R coils are located as close as possible to the model plane because of the high field required from the R coils. The Y coils are at a larger distance on the y axis. The coil configuration is optimum if the return current from the two straight R coil conductors can be placed at a position which does not change the required field. The above requirement is satisfied by the four race-track coils shown in Figure III.8 along with the other coil systems. Figure III.8 lists the dimensions of all coils and shows their locations.

III.5 CROSS COUPLING

An ideal situation for the MSBS would be for all coils to function independently. Unfortunately this is not possible when the model plane pitches, yaws or rolls. Then there are some minor cross couplings and some major cross couplings. When the model is at zero angle of pitch, yaw and roll, there are no cross couplings between any group of coils with any other group of coils. When the model pitches, yaws or rolls cross coupling occurs. For larger angles the cross coupling is larger. Hence the largest angle of pitch, $\pm 30^{\circ}$, will cause

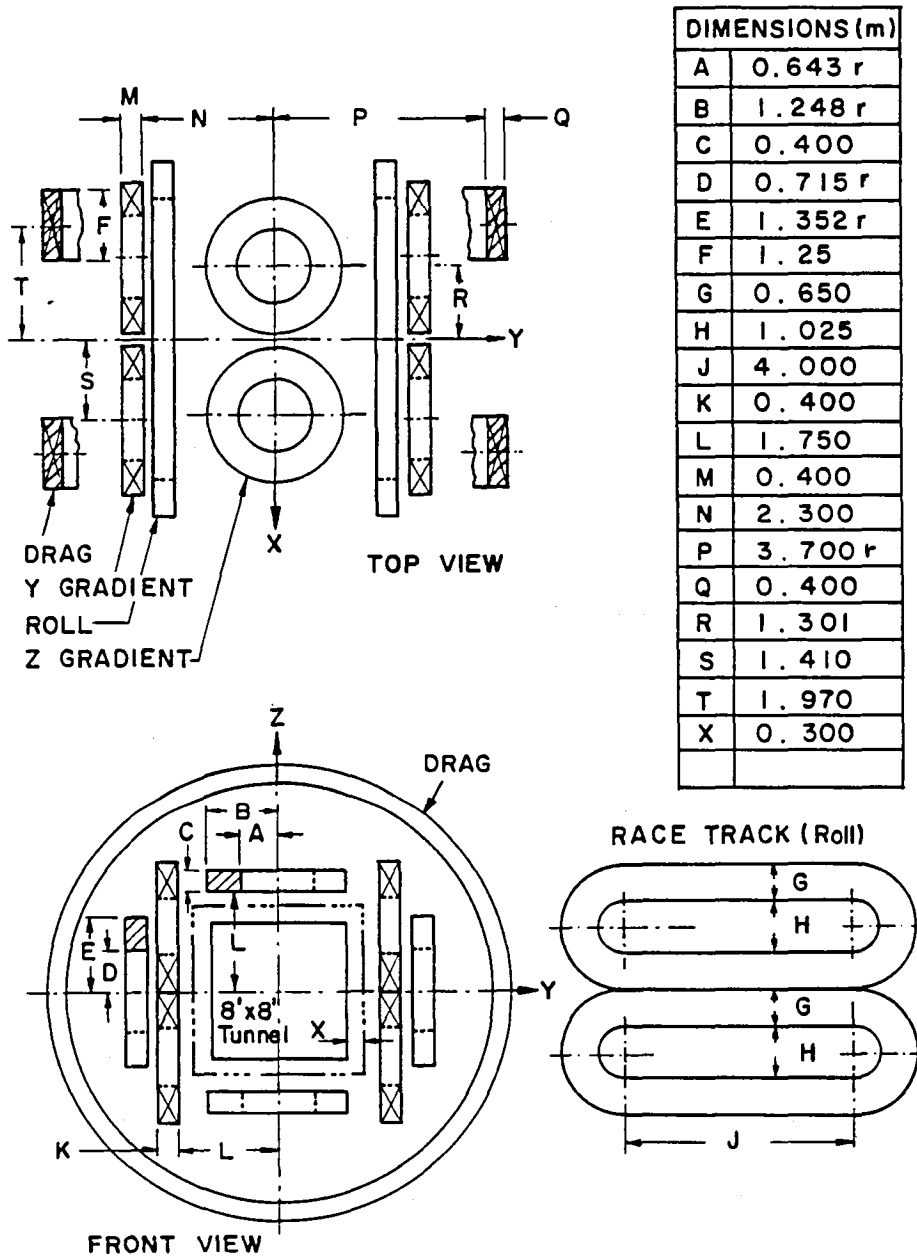


Figure III.8. Magnet System

the highest mode of cross coupling. The roll field is higher than the fields from the X, Y or Z coils because of the very strong fuselage core magnet and the weak wing magnetic core. Consequently, the R coils suffer insignificant cross coupling from the X, Y or Z coils while the latter suffer from the high R coil field. Therefore we emphasize the X, Y and Z coils which are subject to cross coupling from the R coil.

III.5.1 Drag Coils (X Coils)

The drag coils have no cross coupling with the R coils because the main current in the R coils is in the x direction which produces no B_x component. When the model pitches, there is cross coupling between the B_x component from the Z coils and the X coil B_x field. This component may be calculated from $\nabla \times B = 0$. Similarly, as the model yaws, there is cross coupling between the B_x component of the Y coils and the X coil B_x field. Unfortunately, these two cross coupling components act against the required B_x component. At angles α and β in pitch and yaw the B_x component is related to the x, y and z field component of the X, Y and Z coils respectively as

$$B_x = B_{x0} \cos \alpha \cos \beta - B_{y0} \sin \beta - B_{z0} \sin \alpha \quad , \quad (\text{III.8})$$

where B_{x0} is the x component due to the X coils at $\alpha = \beta = 0$

B_{y0} is the y component due to the Y coils at $\alpha = \beta = 0$

B_{z0} is the z component due to the Z coils at $\alpha = \beta = 0$

The required B_x value at maximum pitch and yaw is given in Table II-2.

III.5.2 Z Gradient Coils

When the model pitches or yaws, the total z component at the model tip will be the sum of the z component due to the Z coils, a cross coupling z component from the X coil, and a cross coupling z component from the R coils.

The cross coupling component from the X coil during pitch may be found from $\nabla \cdot B = 0$ and is equal to $-\frac{B_{x0}}{2} \sin \alpha$.

When the model core yaws, the model coil tips experience a B_z component field produced by the R coils. This B_z field from the R coils produces a net F_z force (no pitch torque) on the model core. This force is equal to slightly less than one third of the maximum F_z required on the model. Correction is made by increasing the ampere meters of the Z coils to balance the undesired z force from the R coils. The undesired B_z component during yaw is related to the z component from the R coils at the wing tips, B_{zb} , as

$$B_z = B_{zb} \left(\frac{L}{2b}\right) \sin \beta = 0.128 \sin \beta \quad .$$

In the above equation the maximum value of $B_{zb} = 0.3$ tesla is used.

The total B_z field at angles α and β in pitch and yaw is

$$B_z = B_{z0} \cos \alpha \cos \beta - B_{x0} \frac{1}{2} \sin \alpha + 0.128 \sin \beta \quad . \quad (\text{III.9})$$

In the above equation, cross coupling from the X coils will always strengthen the required B_z component during pitch (positive cross couplings) while the z component from the R coils during yaw may add to or subtract from the net B_z field depending on the angles of roll and yaw.

III.5.3 Y Gradient Coils

There is a positive cross coupling y component from the X coils equal to

$$\left(-\frac{1}{2} \sin \beta\right) B_{x0} \quad .$$

When the model core pitches, the end tips experience a B_y component from the R coil which translates into a net undesired F_y side force. The undesired B_y field component is

$$B_y = B_{zb} \frac{L}{2b} \sin \alpha = 0.128 \sin \alpha \quad .$$

This y component from the R coils causes a serious cross coupling problem; unfortunately there is no apparent solution except for making the Y gradient coils large enough to take care of this undesired field component.

The total required B_y field at angles of α and β in pitch and yaw is

$$B_y = B_{y0} \cos \alpha \cos \beta - \frac{1}{2} B_{x0} \sin \beta + 0.128 \sin \alpha \quad . \quad (\text{III.10})$$

III.5.4 Field Requirement

As discussed in the previous section, the fields B_x , B_y and B_z needed to produce required forces and torques at maximum angular displacement of α , β and ϕ can be expressed in terms of B_{x0} , B_{y0} and B_{z0} as

Eq. III.11

$$\begin{bmatrix} \cos\alpha \cos\beta & \sin\beta & \sin\alpha \\ -\frac{\sin\beta}{2} & \cos\alpha \cos\beta & 0 \\ -\frac{\sin\alpha}{2} & 0 & \cos\alpha \cos\beta \end{bmatrix} \begin{bmatrix} B_{x0} \\ B_{y0} \\ B_{z0} \end{bmatrix} = \begin{bmatrix} B_x \\ B_y - 0.128 \sin\alpha \\ B_z - 0.128 \sin\beta \end{bmatrix}$$

where B_x , B_y and B_z are the field components at the pole tips at angular displacements α and β . B_{x0} , B_{y0} and B_{z0} are the field components at $\alpha = \beta = 0$ due to the X, Y and Z coils respectively. Values of B_x , B_y and B_z at maximum angles ($\alpha = 30^\circ$, $\beta = 10^\circ$) are discussed in Section II.1.3 and listed in Table II-2. Solving the above equation for maximum angles of α and β yields the required maximum field components at $\alpha = \beta = 0$: B_{x0} , B_{y0} and B_{z0} . The solution is

$$B_{x0} = 0.18 \text{ tesla}$$

$$B_{y0} = -0.086 \text{ tesla}$$

$$B_{z0} = -0.159 \text{ tesla}$$

These maximum field components B_{x0} , B_{y0} and B_{z0} are used to size the X, Y and Z coils, respectively. The matrix equation above can be derived from the force relation

$$\vec{F} = (m \cdot \nabla) \vec{B} \quad .$$

IV. MAGNET DESIGN

The magnet system consists of one model superconducting coil, 4 Z gradient coils, 4 Y gradient coils, 2 X drag coils, and 4 R roll coils. The Z, Y, and R coils are fully bipolar while the X coils are monopolar. The symmetry of the coil array enhances the reliability of the magnet system.

IV.1 MAGNET SYSTEM REQUIREMENT

All system requirements discussed in Chapter II for static forces and torques plus the 10 Hz dynamic control forces are met with the system configuration described in Chapter III. Other magnet requirements such as peak magnetic field strength, peak voltage at the magnet terminals and the structure requirements are within the state of the art.

IV.1.1 Coil Shapes

All coils are solenoids except the race track R coils. The use of race track R coils instead of solenoids minimizes ampere meters and stored energy.

IV.1.2 Coil Peak Fields

The maximum field in each coil is found by field scanning the coil with all other coils powered to ± 11 kA. The maximum found may be unrealistically high compared to normal operation. The maximum values for self and total fields are listed in Table IV-1. It is seen that 6.3 T on the Y coil is maximum.

TABLE IV-1
MAXIMUM FIELDS IN COILS IN TESLA

Coil	Self Field Max.	Total Field Max.
R	4.2 T	6.1 T
X	3.8	4.4
Y	4.0	6.3
Z	4.0	5.8

IV.1.3 Coil Terminal Voltages

The requirement for dynamic control is $\pm 0.1\%$ of any magnet current at 10 Hz. Accordingly the maximum voltage across any MSBS coil is about 3000 V on the X coil.

The power supply maximum voltage and power is determined for $I = 11$ kA in all coils and for the 10 Hz correction to be applied to each coil continuously at maximum amplitude. The requirements on power supplies for initial charging to full current in all coils is less than for the 10 Hz load providing the charge time exceeds 25 sec. The 2 min and 10 min charging powers are smaller as seen in Table IV-2.

IV.1.4 Coil Structural Design

The system structure meets all the specified functional requirements with 304 N stainless steel designed at 137.9 MN/m^2 working stress. In lower stress areas 304 and 304 L are used. The system structure provides for and reacts gravity loads, steady state forces and 10 Hz control forces, vacuum pressures, thermal cycling contraction forces, and accurate coil positioning with acceptable flexure during pulsing.

The system structure is the main AC load on the helium system during full load. The internal coil structure is a bifilar 304 stainless steel strip slightly higher than the conductor. All axial forces and all radial forces are taken by this interleaved strip. The forces are spread each layer by radial insulator separator slats.

TABLE IV-2
VOLTAGE AND POWER REQUIREMENTS PER COIL

Coil	10 Hz at 0.1% of <u>max current</u>		2 min charge <u>specification</u>		10 min charge <u>specification</u>	
	Voltage V	Power MW	Voltage V	Power MW	Voltage V	Power MW
Z	131	1.44	27.3	0.30	5.5	0.06
Y	173	1.90	36	0.4	7.2	0.08
X	3018	33.2	629	6.92	125.8	1.38
R	399	4.4	83.5	0.92	16.7	0.19
Total Power*	97.2 MW		20.25 MW		4.08 MW	

*For all coils simultaneously.

IV.1.6 Magnet Control Requirement

The control requirement is 0.1% of the static forces at 10 Hz. Each R, Y and Z magnet has a 3 phase Graetz bridge SCR bipolar power supply with voltages sufficient to provide the 10 Hz current variation for control, see Table IV-2. The X coils are monopolar and require only monopolar power supplies. In all cases the power supply voltage must be sufficient to overcome any unwanted voltage pickup from any other coil undergoing control current correction in addition to providing its own dI/dt .

IV.2 CONDUCTOR

The conductor in all coils is the ANL 11 kA cable conductor.⁽³⁾ The cable was fabricated by Supercon Inc. by twisting 24 basic cables around an insulated stainless steel strip with a twist pitch of 22.5 cm. A photo of the cable is shown in Fig. IV.1. The basic cable is made by twisting three, seven-strand conductors (triplex cable) with a twist pitch of 2.2 cm. The seven-strand conductors are made of six OFHC copper wires twisted around a superconducting center conductor and soldered with Staybrite. Since the requirements of low AC losses and cryostability conflict with each other, the basic principle chosen is to achieve cryostability within the basic cable. To restrict AC coupling among the 24 triplex cables in the final cable, only limited current sharing among the triplex is allowed by coating a thin insulating film around the seven-strand conductors. Each superconducting strand has a diameter of 0.051 cm and contains 2041 filaments of 6 μm dia with a twist pitch of 1.27 cm. The copper-to-superconductor ratio for each strand is 1.8.

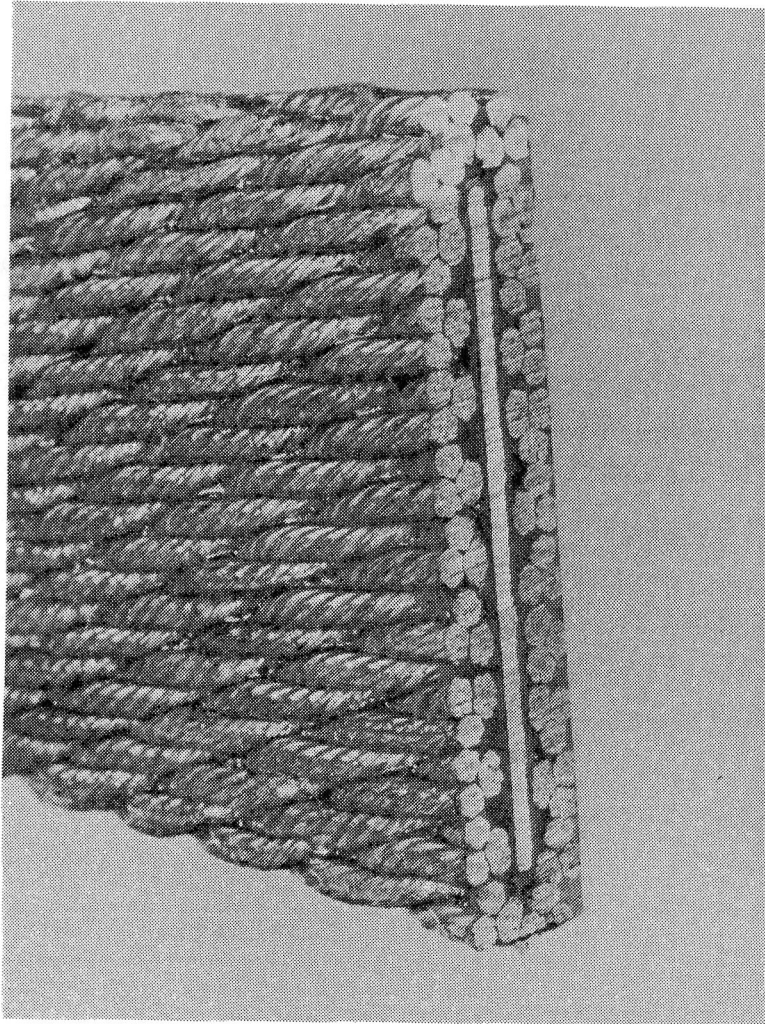


Fig. IV.1 Cryostable 11 kA AC cable.

The final cable is compressed during the cabling by heavy rolls from four sides. This minimizes mechanical perturbations of the basic conductors during pulsing. The compression did not damage the insulation between the 0.1 cm stainless steel strip and the 24 triplex cables. However, owing to the deformation of the soft solder in the seven-strand conductor, about 5% degradation of the recovery current occurs. The MSBS magnet design with interleaved 0.19 cm to 0.53 cm thick stainless strips between turns relieves

the necessity to square up a winding with accurate cable compression since the strips, not the cable, govern the winding. The finished cable has a width of 3.78 cm and a thickness of 0.74 cm.

Conductor coils were pulsed up to 11 T/s with relatively low losses. After more than 4000 pulsing cycles, no changes in the pulsing characteristics and cryostability of the coil were observed. Thus the 11 kA cable is an ideal conductor for all MSBS coils. In the ANL 1.5 MJ coil the gross current density was 2300 A/cm². For the MSBS coils a current density of 1500 A/cm² will be used, which is more conservative and allows space for extra stainless steel interleaved banding.

An extra 25% NbTi over the above design is allowed to provide extra stability margin. This additional NbTi is included for cost estimating in Chapter VIII.

IV.2.1 Conductor Cooling and Stability

The MSBS magnet system is pool cooled with saturated liquid helium at 4.2 K, which is most common for large modern superconducting coils. With pool boiling the conductor is cooled by natural convection. A typical gross current density for large coils in 4.2 K Helium I is 1500 A/cm². The heat removal to helium and by end cooling of a short normal region is equal to heat generated when normal. Other cooling schemes such as supercritical helium or superfluid helium (Helium II) offer higher current densities or higher fields or both. For the MSBS system an improvement in current density would provide higher fields at the model with less NbTi in all coils. This could provide either significant cost reduction or performance improvement with identical coils. Helium II usage deserves further analysis.

IV.3 MAGNET SYSTEM CONCEPT

The magnet system configuration is shown in Fig. III. 7. The system consists of 14 superconducting coils arranged around the tunnel test section. The function and arrangement of these coils is discussed in detail in Chapter III. All the coil forms are slotted stainless steel with epoxy plate reinforcement. The forces and torques between the coils are contained by cold stainless steel structure with a special design to minimize structural eddy current losses in the drag coils as well as with general slotted forms for all coils. Details of the dewar and structure are in Chapters V and VI.

IV.3.1 System Analysis

The computer code EFFI⁽⁵⁾ is used to calculate magnetic fields, forces, torques, field profiles in the tunnel area, and coil inductances.

Magnetic forces are calculated for all coils in the system under maximum static forces and moments and different modes of operation. The analysis shows the need for rigid, bi-directional coil supports.

The homogeneity of the magnetic fields in the model region is examined in detail. Cross coupling between the different coils at different modes of operation is accounted for as explained in the previous chapter.

The self and mutual inductances of the MSBS coil system are calculated with the computer program EFFI. The inductance matrix is shown in Table IV-3. The mutual inductances between coils are relatively small compared to self inductances, except for the large coupling between the Y gradient coils and the race track R coils.

TABLE IV-3
INDUCTANCE MATRIX IN MILLI HENRIES

	Z	Z	Z	Z	Y	Y	Y	Y	X	X	R	R	R	R	
	1	2	3	4	5	6	7	8	9	10	11	12	13	14	
1	200														Top Front
2	8	200													Top Rear
3	3	1	200												Bottom Front
4	1	3	8	200											Bottom Rear
5	5	1	5	1	250										Right Front
6	1	5	1	5	10	250									Right Rear
7	5	1	5	1	2	1	250								Left Front
8	1	5	1	5	1	2	10	250							Left Rear
9	16	17	16	17	29	26	29	26	5,581						Front
10	17	16	17	16	26	29	26	29	893	5,581					Rear
11	15	15	5	5	4	4	28	28	52	52	594				Left Top
12	5	5	15	15	4	4	28	28	52	52	76	594			Left Bottom
13	15	15	5	5	28	28	4	4	52	52	19	9	594		Right Top
14	5	5	15	15	28	28	4	4	52	52	9	19	76	594	Right Bottom
	297	297	297	297	394	394	394	394	6,858	6,858	906	906	906	906	19,520

Number of Turns:
 Z-Coil = 330
 Y-Coil = 346
 X-Coil = 682

IV.3.2 Model Core Solenoid

The model core solenoid is maximum length and maximum diameter to achieve the highest possible magnetic moment and pole strength. The solenoid is a high performance persistent epoxy potted solenoid 70 cm long and 11.5 cm OD wound with 10 A composite NbTi wire. A small prototype model core superconducting coil has been successfully tested under wind tunnel operating conditions by Britcher, Goodyer, Scurlock and Wu at Southampton University.⁽⁶⁾ Table IV-4 lists coil parameters.

Potted (epoxy impregnated) coils are adiabatically stable. Such coils do not contain much copper or cooled surfaces, and their ability to tolerate disturbances is limited to the adiabatic heat capacity of the conductor material. However the absence of large amounts of copper and helium in the windings allows such coils to operate at current densities up to ten times as large as those for cryostable coils which is ideal for model cores. Based on General Electric experience and technology,⁽¹⁾ a field of 6.1 tesla and current density of 30,000 A/cm² is used.

The cryostat is shown in Fig. IV-2. The internal cold dewar is supported at each end by fiberglass epoxy support loops from a S.S. support plate which is cooled by a 6.35 mm OD helium vent tube which is wrapped into a helix to extend its heat transfer length before exiting at the rear into the wind tunnel. The intermediate shield temperature is approximately 75 K. The internal cold dewar is supported from inset axial G-11 tubes at each end to reduce the heat leak into the dewar.

The helium capacity is 3.5 liters, the idling boil off rate is 0.137 l/h, and the idling time to lose 50% helium is 10 hours. For an expected AC 10 Hz

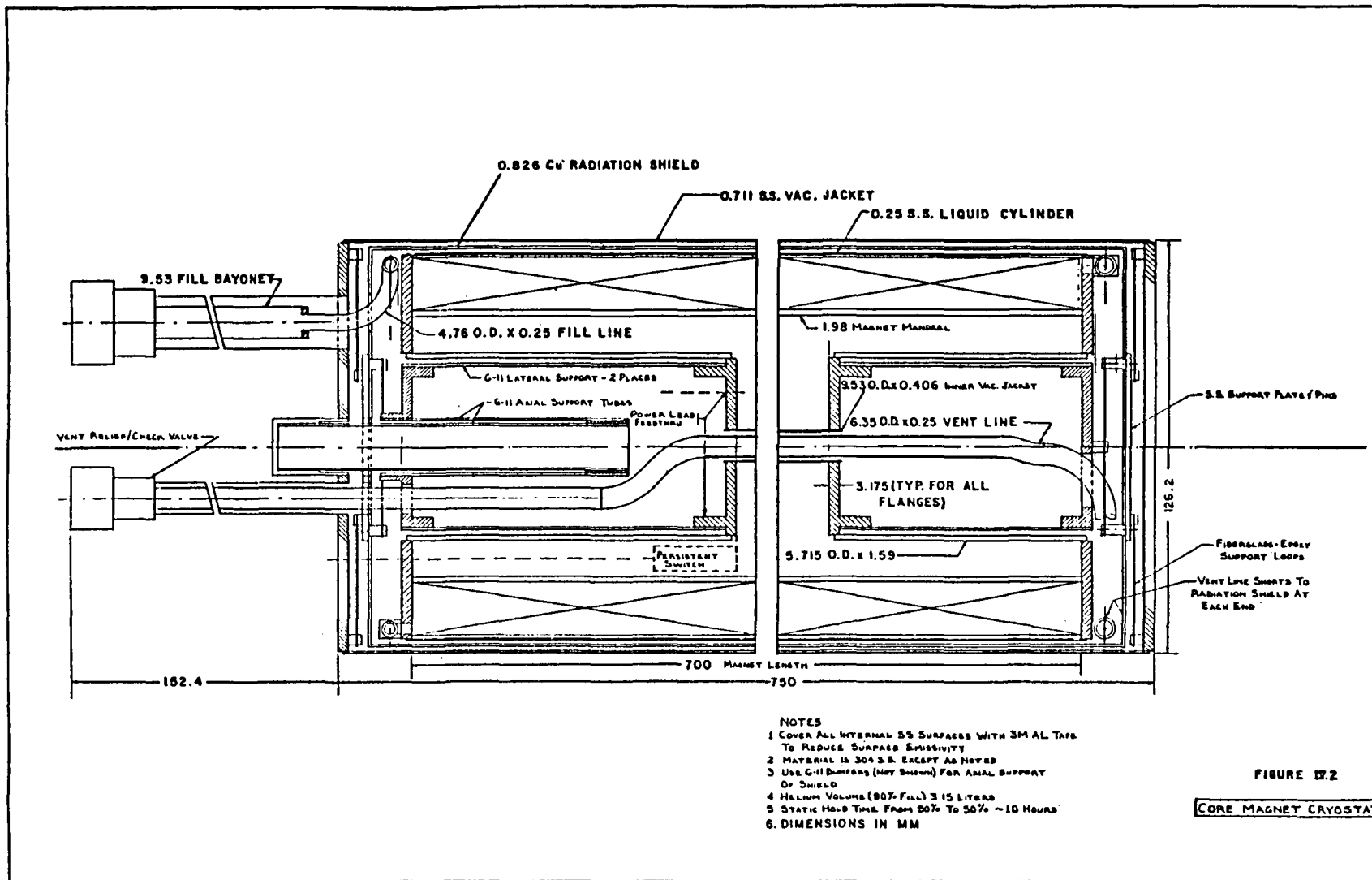


TABLE IV-4

MODEL COIL PARAMETERS

Length (cm)	70
OD (cm)	11.5
ID (cm)	8.26
Operating Current (A)	10
Winding Current Density (A/m ²)	3×10^8
Peak Field (T)	6.1
Stored Energy (MJ)	0.065
Number of Turns	339,780
Conductor Length (m)	1.055×10^5
Conductor Diameter (cm)	0.02
AC Losses at full load (W)	~ 0.03

TABLE IV-5

X DRAG COIL PARAMETERS

Number of Coils	2
Number of Turns/Coil	682
Bifilar S.S. Strip Width (cm)	0.53
Operating Current (kA)	11
Winding Current Density (A/cm^2)	1500
Peak Field (T)	4.4
Height (m)	1.25
O.D. (m)	8.2
I.D. (m)	7.4
Energy Stored/Coil (MJ)	328
Inductance (H)	5.58
Voltage for 10 Hz (V)	1509
AC Losses/Coil at 10 Hz (W)	99.2
Discharge Voltage (kV) ($T_{max} \sim 200$ K)	1.05

TABLE IV-6

Y GRADIENT COIL PARAMETERS

Number of Coils	4
Number of Turns/Coil	346
Bifilar S.S. Strip Width (cm)	0.24
Operating Current (kA)	11
Winding Current Density (A/cm ²)	1500
Peak Field (T)	6.3
Height (m)	0.4
O.D. (m)	2.7
I.D. (m)	1.43
Energy Stored/Coil (MJ)	15.3
Inductance (H)	0.251
Voltage for 10 Hz (V)	86.4
AC Losses/Coil at 10 Hz (W)	11.4
Discharge Voltage (kV), ($T_{\max} \sim 200$ K)	0.67

TABLE IV-7

Z GRADIENT COIL PARAMETERS

Number of Coils	4
Turns/Coil	330
Bifilar S.S. Strip Width (cm)	0.24
Operating Current (kA)	11
Winding Current Density (A/cm ²)	1500
Peak Field (T)	5.8
Height (m)	0.4
O.D. (m)	2.486
I.D. (m)	1.286
Energy Stored/Coil (MJ)	12.3
Inductance (H)	0.21
Voltage for 10 Hz (V)	65.4
AC Losses/Coil at 10 Hz (W)	9.8
Discharge Voltage (kV), ($T_{\max} \sim 200$ K)	0.56

TABLE IV-8

R COIL PARAMETERS

Number of Coils	4
Turns/Coil	355
Bifilar S.S. Strip Width (cm)	0.19
Operating Current (kA)	11
Winding Current Density (A/cm^2)	1500
Peak Field (T)	6.1
Energy Stored/Coil (MJ)	35
Inductance (H)	0.588
Voltage for 10 Hz (V)	200
AC Losses/Coil at 10 Hz (W)	30.4
Discharge Voltage (kV), ($T_{max} \sim 200$ K)	0.79

loss of 0.03 W at full load the time to 50% helium boil off would be about 7 hours. A battery powered liquid level sensor is feasible but requires either radio or optical transmission.

IV.3.3 X, Y, Z and R Coils

The specifications for the X, Y, Z and R coils are listed in Tables IV-5, 6, 7 and 8. Note that most of the energy is stored in the X coils, where more internal structure bifilar S.S. strip is needed. The ampere meters and stored energy are listed in Table IV-9.

TABLE IV-9
AMPERE METERS AND STORED ENERGY

Coils	4R	2X	4Y	4Z	Total
Ampere Meters (MAm)	207	362	100	86	755
Stored Energy (MJ)	140	656	60	50	906

The coil weights are divided between the interleaved stainless steel strip, 0.53 cm to 0.19 cm thick, and the conductor shown in Fig. IV.1 which includes a 0.1 cm strip of internal stainless steel. The weights are listed in Table IV-10.

TABLE IV-10
COIL WEIGHTS, kg

Coils	R	X	Y	Z
Conductor	6240	21,700	3000	2580
S.S. Strip (width cm)	2860 (.19)	27,700 (.53)	1740 (.24)	1510 (.24)
Total	9100	49,400	4740	4090
No. Coils	4	2	4	4
Total Weight (kg)	36,400	98,800	18,960	16,360
Sum	170,520 kg			

The AC losses in the coils and stainless steel structural interleaved strip at 10 Hz for full and quarter load are listed in Table IV-11. Hysteresis for the 6 μm filaments of NbTi is the major loss item. At quarter load hysteresis is only about half the value at full load while the other eddy current losses are 1/16 down.

The eddy current losses into the liquid helium from 10 Hz AC induced current in nearby cold S.S. heavy structures are the major operating losses for the cryogenic system. The large X coils are entered as zero loss in Table IV-12 because of the complete cold structural slot in the structure, as explained in Chapter V. X coil structural losses are not exactly zero because all nearby small webs and flanges try to shield their own volume. Such detailed calculations were not undertaken and are expected to be small.

A major potential loss is due to the presence of the inner cold S.S. surfaces of the X coil. Although these surfaces are split as explained above to avoid direct coupling with the X coil windings such surfaces still couple to all other coils. To the R, Y, and Z coils the inner heavy surfaces of the X coils, on which the X turns are wound, appear as large, thick flat plates. The losses listed in Table IV-12 assume that these plates are segmented to avoid such losses. It is beyond the scope of this report to present this detailed design which is a difficult electrical and mechanical compromise in a high stress structural region. Additional assistance is expected from taking advantage of the higher stress rating for stainless steel at low temperature which could reduce some thicknesses as discussed in V.2. For example at 10 Hz reducing plate thicknesses to one-half would reduce power losses by one-half, even without segmenting.

TABLE IV-11
COIL AC LOSSES AT 10 Hz

Coil	R	X	Y	Z	Sum
Hysteresis	27.7	80.0	10.35	8.9	
Conductor	2.3	8.2	0.8	0.7	
S.S. Strips	.44	11.0	0.22	0.2	
Total	30.4	99.2	11.4	9.8	
No. Coils	4	2	4	4	
Total, Full Load	121.6	198.4	45.6	39.2	405 W
Total, Quarter Load	56.1	92.0	22.2	19.1	189 W

TABLE IV-12
EDDY CURRENT LOSSES IN THE EXTERNAL STRUCTURE
FOR 10 Hz CONTROL AT 0.1% I

Coils	Power Loss at Full Load	Power Loss at 1/4 Load
R	676 W	42.3 W
X	--	--
Y	600	37.5
Z	284	17.8
TOTAL	1560 W	97.6 W



V. STRUCTURAL AND THERMAL DESIGN

V.1 INTRODUCTION

There are three structural design drivers:

- Size and location of the magnets
- Magnet forces and torques
- Choice between individual cryostats or one common cryostat.

These three factors are inter-dependent with the objective of making the magnets small and locating them as close as possible to the model in the wind tunnel. It is found that the magnet coils can be located closer to the tunnel and closer to each other if they share the same pool boiling helium enclosure. There is a significant thermal advantage for transferring inter-magnet forces directly through cold structure in a common cryostat as compared to transferring inter-magnet forces from cold to warm and back to cold. Thus all of the magnets are housed in a single primary helium reservoir attached to a single cold structure frame except the drag coils which have separate liquid containers.

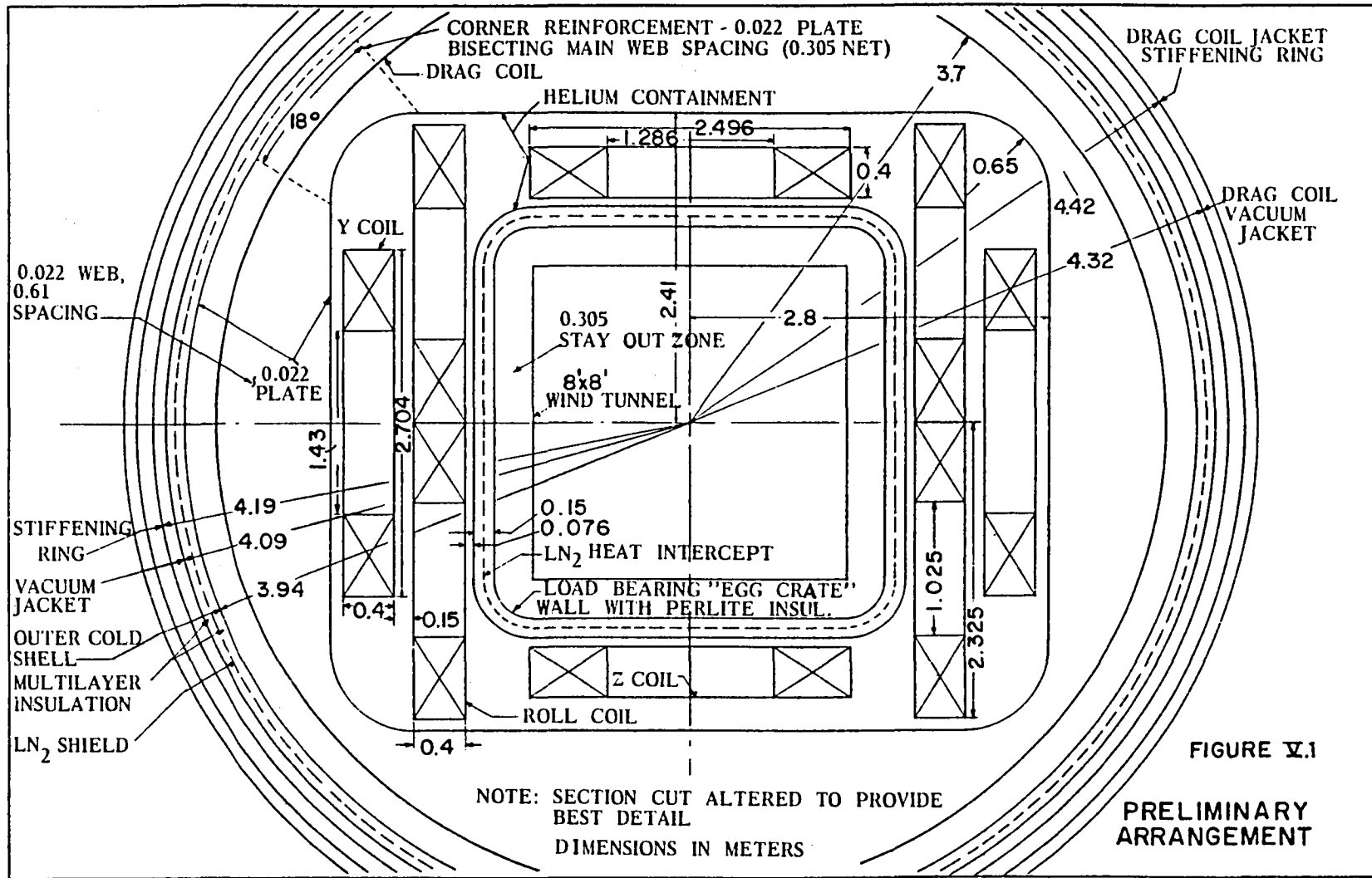
The selected design includes a load-bearing thermal-vacuum enclosure immediately surrounding the wind tunnel, a large rectangular box with rounded corners for mounting the R, Y and Z coils, the principal structural elements which incorporate the two large X coils, a cylindrical outer cold surface, multilayer insulation space with liquid nitrogen shield, and the stiffened outer vacuum jacket. To reduce eddy current losses in the X coils the entire cold structure has a longitudinal electrical break. The helium container around each X coil is a thin non-structural stainless steel liner which

includes a separate electrical break. The use of a thin liner to contain helium removes the requirement to seal against helium leakage at insulated flanges in the heavy structural walls which are subject to large mechanical torques.

Several drawings and sketches made in the course of the design study provide a physical understanding of the system. The first of these, Fig. V.1, is a simplified section of the wind tunnel and cryostat which shows the general arrangement of the system and the location of the Y, Z and R coils. Location of the X coils is less clearly depicted. The next drawing, Fig. V.2, is a first attempt to show an isometric view of the basic cryostat. While the main portion of this drawing is not particularly informative, the location and size of the Drag coils is shown. More information is provided in the smaller longitudinal section quadrant view since it shows a drag coil, location of the structural webs, and the scheme for connecting the load bearing "egg crate" structure with the main part of the cryostat. The best view of the relative sizes and positions of the magnets in the cryostat is shown in Fig. V.3 which is entitled, "Cryostat Cut Away Isometric." Finally, Fig. V.4 shows two views of the complete cryostat and its support system in place around the wind tunnel. Other smaller sketches have been prepared to support description of specific features discussed in the following sections.

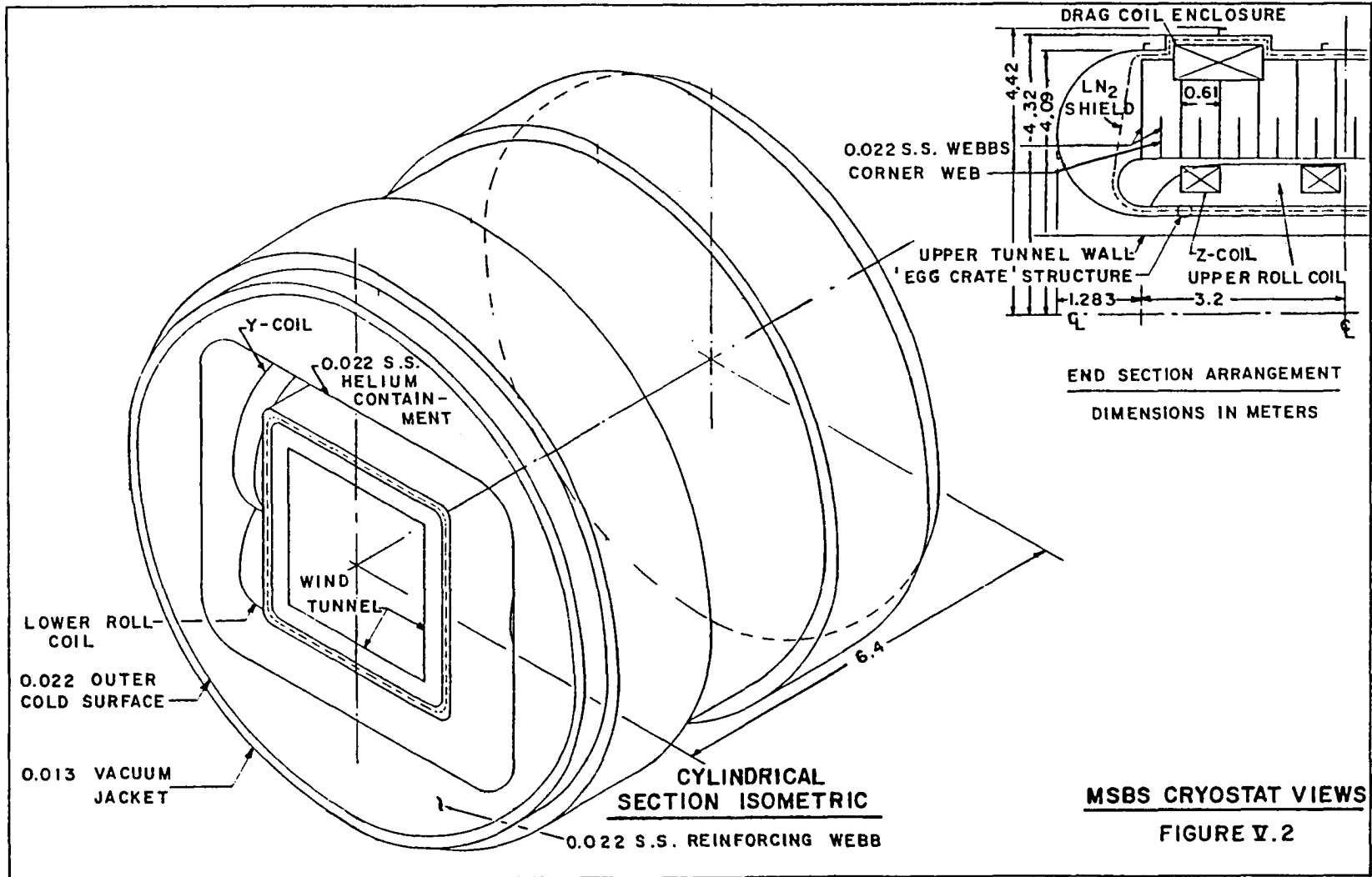
V.2 MATERIALS

Structural and thermal design is based on materials satisfactory for use at low temperature in high magnetic fields. The list is not extensive. 304 N



NOTE: SECTION CUT ALTERED TO PROVIDE BEST DETAIL
 DIMENSIONS IN METERS

FIGURE V.1
 PRELIMINARY ARRANGEMENT



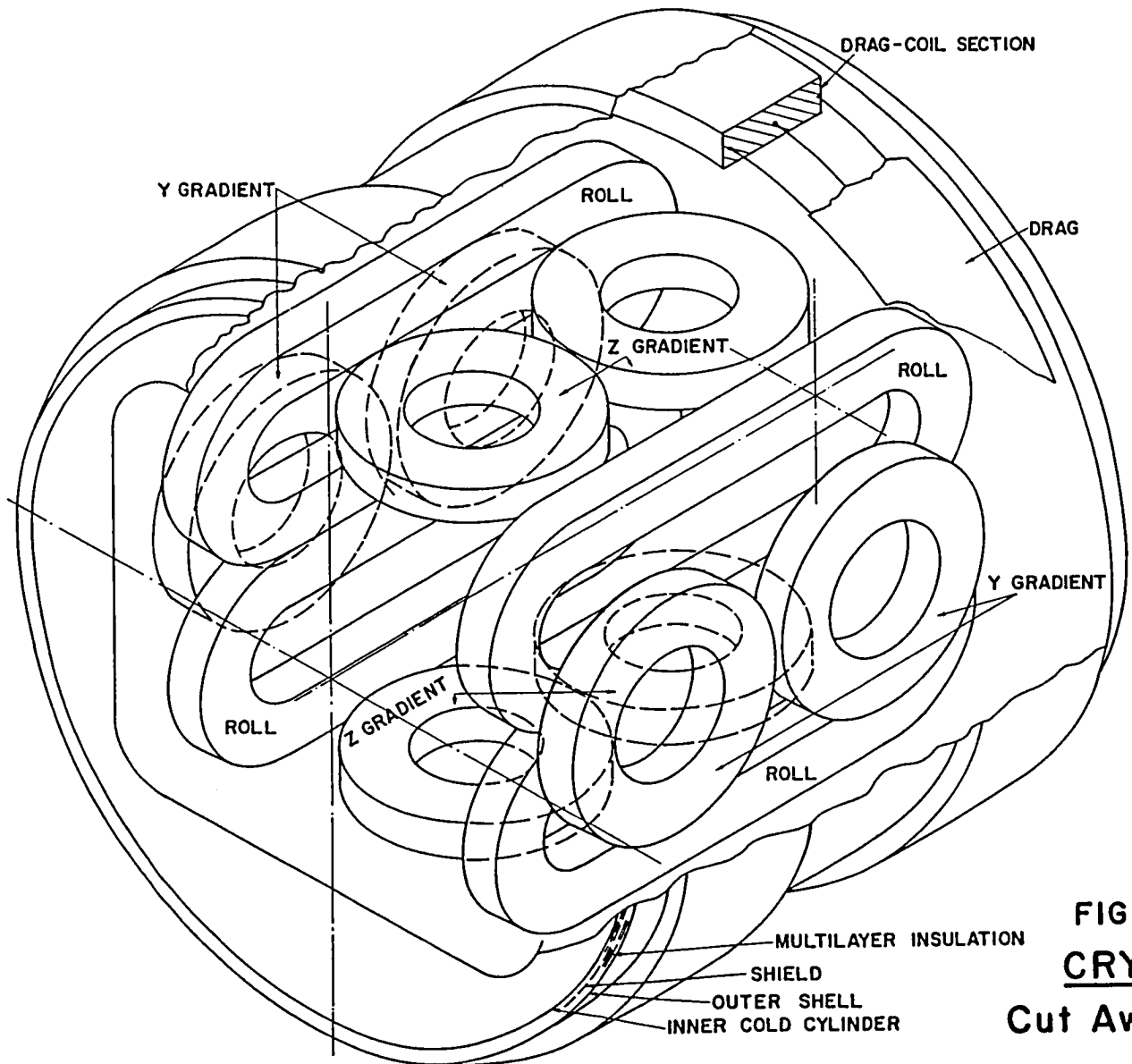


FIGURE V.3
CRYOSTAT
Cut Away Isometric

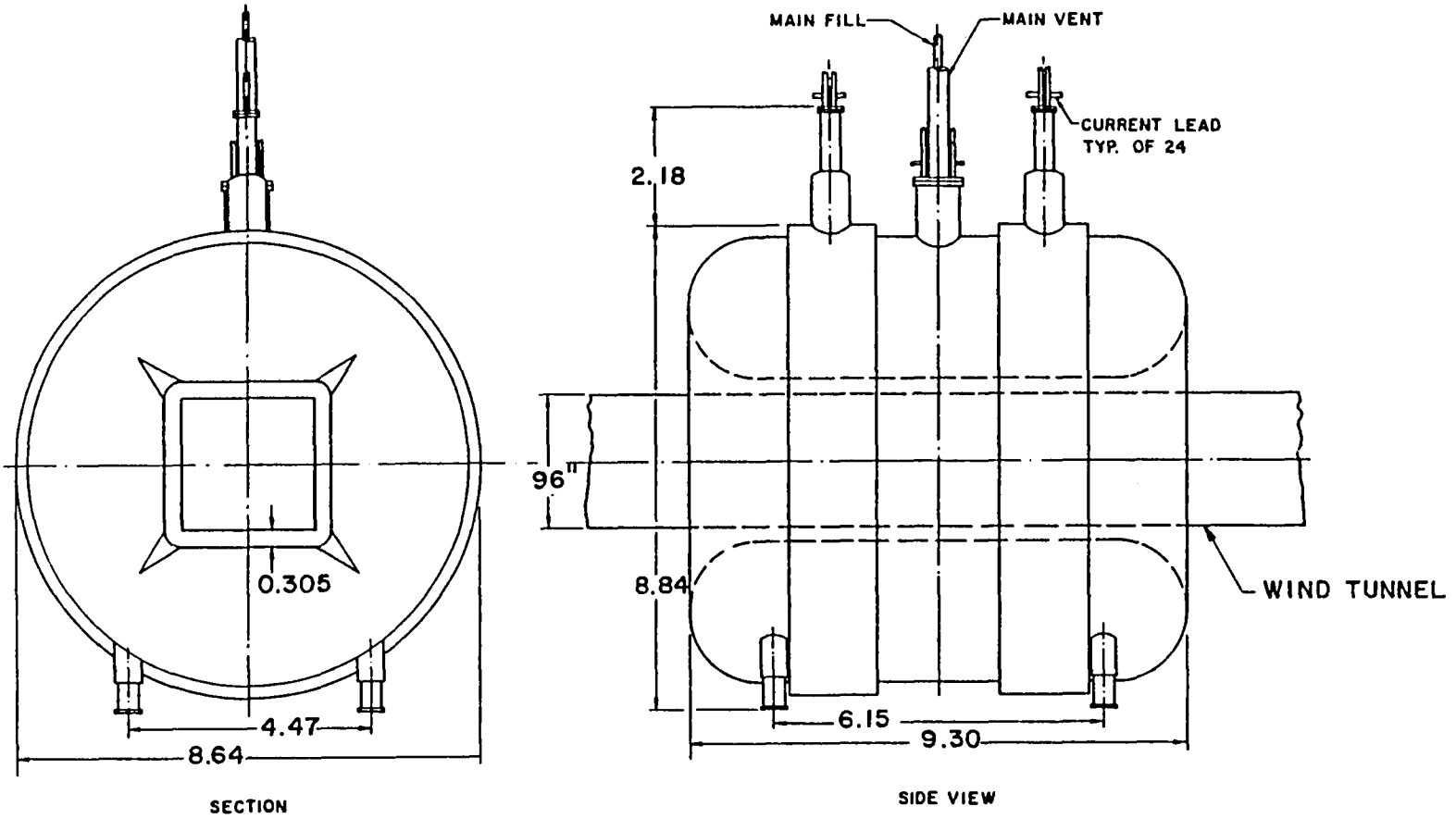


FIGURE V.4
MSBS GENERAL ASSEMBLY
 DIMENSIONS IN METERS

NOTE: NOT ALL DETAILS SHOWN DUE TO SCALE LIMITATIONS

stainless steel is the main structural material of the cryostat. 304 or 304 L are used as convenient in lower stress areas. Liquid nitrogen thermal radiation shields are ETP copper with 1100-0 aluminum sheet and tube as an alternate. G-11 CR epoxy-fiberglass composite is the material used for cryostat supports, for clamp plates on the individual magnets and for electrical insulation and separation between structural sections. Structural bolts are a nickel-manganese alloy, Nitronic 40. 2024-T6 or 7075-T6 aluminum alloy rods may be used to clamp the magnet coils together, since relative contraction is favorable.

Room temperature properties are used for mechanical design even though the selection of materials primarily depends on low temperature suitability. This may be overly conservative for the 304 N cold structure since magnetic forces can only exist when the cryostat is filled with liquid helium. The ultimate tensile strength of annealed stainless steel typically increases by about a factor of three in cooling from ambient to 4.2 K. Thus, it is possible to design structure based on higher maximum stress values which would result in mass and cost reductions. These possibilities warrant further structural analysis. Thinner sections, by the factor of three, are used in critical regions to reduce AC losses, see Table IV-12. However, for this study the following properties are used for mechanical design:

304 N - Suitable for low temperatures and used in large magnet cryostats at Lawrence Livermore Laboratory. ASME design stress of 137.9 MN/m^2 .

304 and 304 L - These stainless steels are not specifically used in the design but may be used where stress is not critical. ASME allowables for

304 and 304 L are 129.6 and 108.25 MN/m² respectively.

Nitronic 40 - The ASME equivalent of this material, UNS S21904, has an allowable design stress of 155.13 MN/m² and it is suitable for low temperatures. Nitronic 40 would be used for structural bolting.

ETP Copper - Electrolytic Tough Pitch copper is a common commercial material with high thermal conductivity. It is easy to solder and silver braze but is not satisfactory for welding. Since only de-oxidized copper can be welded and cycled to low temperature more expensive OFHC copper will be used.

1100 Aluminum - If extensive shield welding is required, 1100-0 aluminum may be used. The disadvantage of aluminum is that the trace tubes carrying liquid nitrogen are more difficult to solder and join than copper.

G-11 CR - This material is the premium commercial epoxy-fiberglass composite for low temperature applications. It has low thermal conductivity and good strength with design allowables between 103.4 and 137.9 MN/m² depending on the application.

2024-T6 or 7075-T6 - These heat-treatable aluminum alloys have high strengths at low temperature. They are good candidates for magnet clamp bolts because their thermal expansion coefficients are nearly 50% greater than stainless steel which causes such bolts to tighten on cool down and their low tensile modulus of 72,395 MN/m² makes them "springy" in relation to stainless steel.

V.3 FORCES AND TORQUES

The interactive resultant forces on each magnet are computed with the EFFI code. These forces and torques are given in Table V-1 for simultaneous maximum loadings. This loading assumption may be overly stringent and a careful analysis of the maximum realistic combination of loadings should be a part of future design work since any reduction will result in less expensive structure.

Eddy current forces between magnets and external structure are much smaller than the magnet to magnet forces, see Table V-2. The eddy current forces are found by computing the mutual energy between coils and nearby plates and differentiating that energy term. The X coils do not produce eddy current forces because they are completely surrounded by liners and structure with electrical breaks. However, a more careful but complex calculation would give forces from several webs and arcs of S.S. around the X coils even if the complete secondary circuit has been eliminated.

V.4 STRUCTURAL DESIGN

The first step in structural design is to determine how close to the wind tunnel the magnets can be located. This results in the selection and design of the load bearing "egg crate" wall around the tunnel. This evacuated and insulated structure supports atmospheric pressure on the wind tunnel side and the static plus overpressure of liquid helium on the other side for a differential on the order of 0.14 atm. This is accomplished in a structure only 152.4 mm thick without protruding beams. The egg crate name stems from the design which consists of 2 mm (14 gauge) stainless steel skins

TABLE V-1
COIL FORCES AND TORQUES*

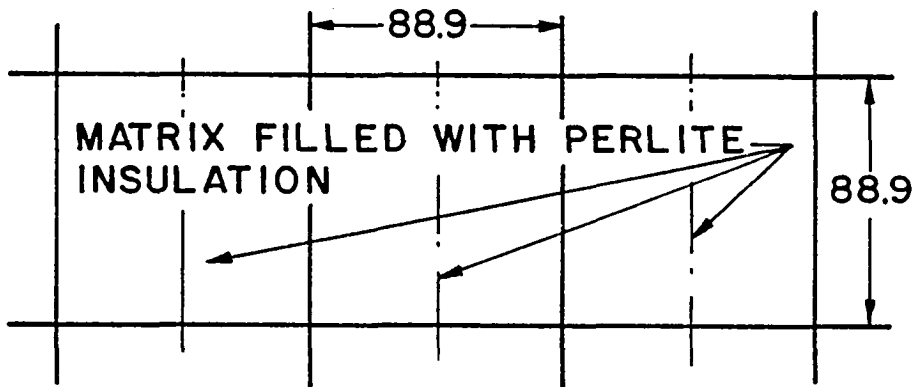
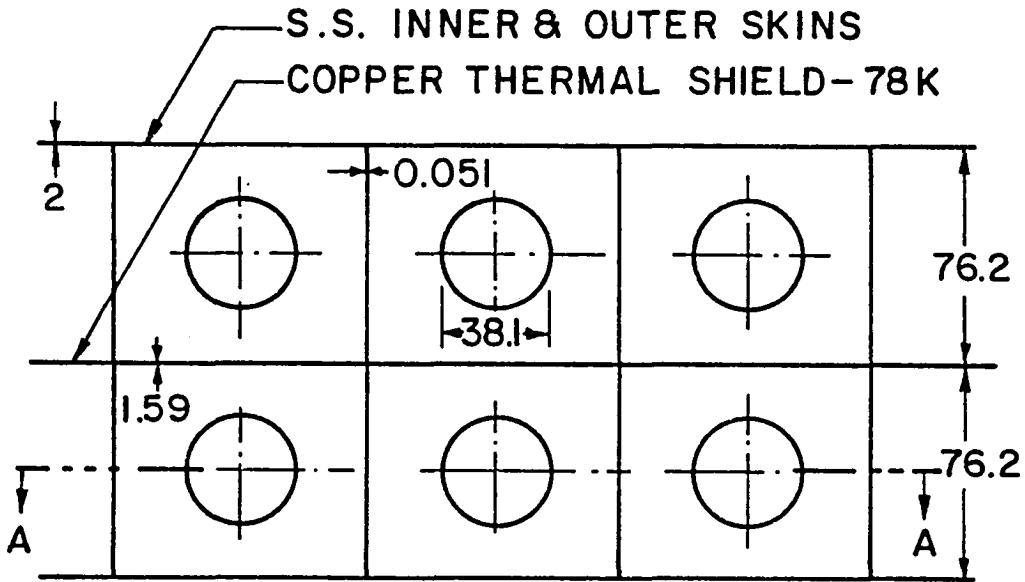
Coil	F_x MN	F_y MN	F_z MN	T_x MN-m	T_y MN-m	T_z MN-m
Z	± 5.9	± 6.0	± 7.0	± 8.0	± 26.3	0
Y	± 9.0	± 5.8	± 23.4	± 8.6	0	± 25.7
X	± 60.0	± 9.1	± 8.0	0	± 44.6	± 63.7
R	± 5.9	± 15.3	± 42.6	± 27.2	± 41.1	± 71.0

*Based on R coil pairs being series connected.

TABLE V-2

EDDY CURRENT FORCES BETWEEN STRUCTURE AND COILS
AT FULL LOAD

Coil	Outer Plate 22.23 mm	Inner Plate 2 mm	Drag Coil Shell 22.23 mm
Z	4.44 kN	0.82 kN	1.06 kN
Y	10.72	0.16	1.48
R	8.14	0.94	1.56
X	$\cong 0$	$\cong 0$	$\cong 0$



VIEW A-A

DIMENSIONS IN MM

FIGURE V.5

EGG CRATE DESIGN SCHEMATIC

supported by a 88.9 mm square matrix of 0.051 mm G-11 CR sheet similar to an over-size honeycomb structure. A sketch of the egg crate structure is shown in Fig. V.5. The configuration of the egg crate inner wall provides a physical reference point for the magnet coil system design. Following the magnet design it is possible to size the enclosure. Structure design follows from the above coil configuration and forces and torques listed in Table V-1. Stress calculations are made in three dimensions for what appears to be worst case combinations of forces and torques. The resultant structural scheme is illustrated in Fig. V.1 and Fig. V.2. As shown, the structure is basically a continuous flange I beam with repeating variable depth webs spaced 609.6 mm on centers. Additional webs are inserted in the corner areas to increase the section modulus of the equivalent fixed-end beams. The design utilizes 22.23 mm thick 304 N plate throughout with all stresses less than 137.9 MN/m^2 .

Although the stress calculations are done in considerable detail, this work is preliminary and should be considered as an area for additional work. Factors to be considered in the future include:

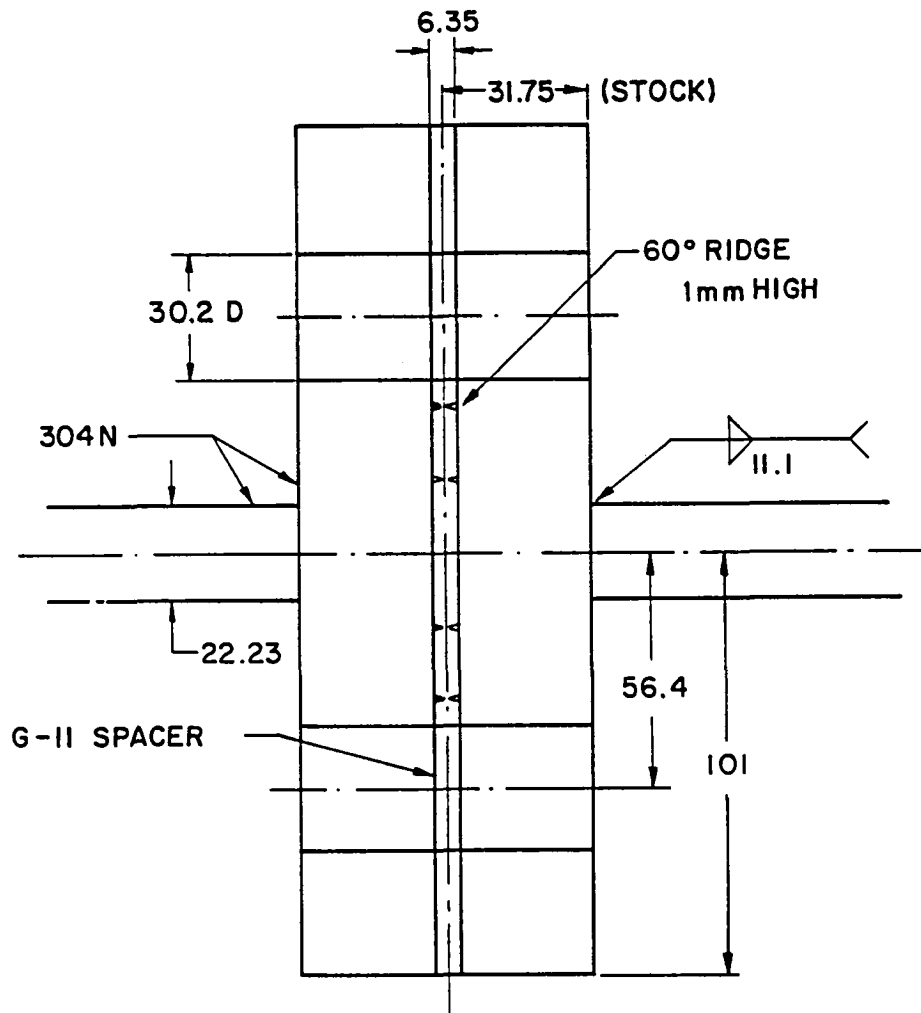
- Re-examination of magnet loads for the most realistic combinations.
- Possible use of 304 N at a higher stress level than 137.9 MN/m^2 .
- Detail design of the internal magnet supports to accurately and effectively distribute loads to the internal rectangular cold surfaces.
- Consider more efficient, alternate structural concepts. The present rectangle in a circle concept is now selected to get structure close to the magnets and to minimize the quantity of contained helium.
- Accurately check the design via a detailed stress analysis utilizing finite elements.

V.5 ELECTRICAL ISOLATION

Structural eddy current helium losses due to the 10 Hz control requirement impose severe thermal loads, particularly due to the Drag coils. This results in the decision to split the entire structure to achieve an open circuit condition for drag coil structural secondary circuits. The split is made at the bottom center of the cryostat where the stress is lowest. Concept designs of the electrical break for the main structure and egg crate cold wall are shown in Fig. V.6 and Fig. V.7.

There are two electrical breaks around the Drag coils. The outer break is purely structural and does not require either vacuum or helium tightness. This break employs a flange similar to that shown in Fig. V.6. The inner break is in the thin stainless steel liner which surrounds each Drag coil and bears against the outer structure. This break must be helium-tight and may employ a flange similar to Fig. V.7. However, even this small flange uses more space than desired so a flat tongue and groove design should be developed for this combination seal and electrical break.

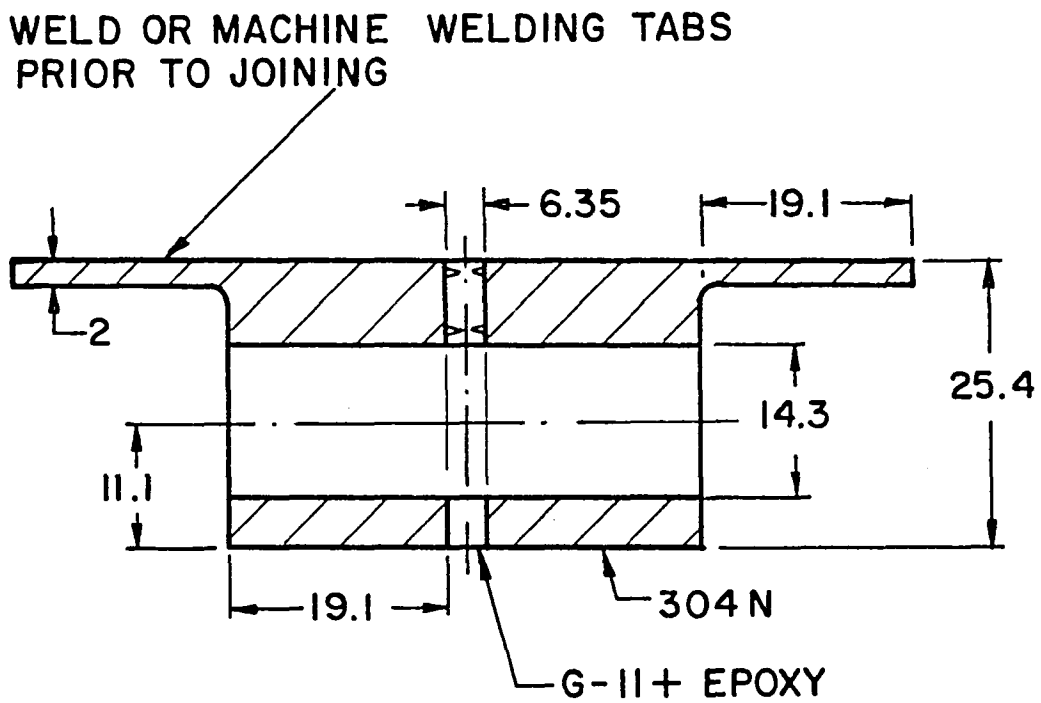
All of the seals utilize epoxy adhesive and fiberglass-epoxy composite insulation and spacer material. The seals are under compression in all cases so that their only function, except for the Drag coil structural break, is to hold liquid helium. This is a high reliability application but it should be pointed out that epoxy composites slowly diffuse helium gas, particularly when warm. Therefore, we would expect to run a small vacuum pump continuously to avoid degradation of the insulating vacuum.



Dimensions in MM.

FIGURE V.6

**BOTTOM PLATE SEAL & ELECTRICAL
INSOLATOR**



Dimensions in MM.

FIGURE V.7

EGG CRATE SEAL & ELECTRICAL
LINER INSULATOR

V.6 WEIGHT SUMMARY

Estimated weights of magnets and structure are given in Table V-3. The estimated total weight of 367,636 Kg falls within a range of + 10% to - 20% which recognizes some overestimate on attachment and clamp structure.

V.7 CRYOSTAT SUPPORT

No additional internal structure is required for mounting since the cryostat structure is very rigid in order to contain the magnetic forces. The design consists of a 1219.2 mm long flat pad for each leg to distribute loads into three main and two partial internal webs. The general arrangement is sketched in Fig. V.8. The support members are four G-11CR tubes 304.8 O.D., 279.4 I.D., and 914.4 mm effective length. Compressive stress per leg is about $75,842 \text{ MN/m}^2$. To account for inward shrinkage of the cold structure, amounting to about 10.7 mm per leg, the legs will be jacked out about 5.35 mm at assembly and will pass through neutral to a similar 5.35 mm cold deflection. Maximum bending stress in the legs due to these deflections will be about 50.33 MN/m^2 . These legs cannot withstand a 1/2 g seismic load, $M = 0.41 \text{ MN-m}$, and will require diagonal tension braces of unidirectional fiberglass-epoxy or aircraft cables.

Both the legs and seismic braces have liquid nitrogen heat intercepts to limit helium heat leak. Estimated heat leak of the entire support assembly is:

<u>Helium</u>	<u>Nitrogen</u>
2.36 W = 3.33 L/h	17 W = 0.4 L/h .

TABLE V-3
ESTIMATED WEIGHTS OF MAGNETS AND STRUCTURE

Main cryostat stainless steel structure	127,834	kg
End bells	9,636	
Egg crate assembly	4,727	
LN ₂ shield assembly	2,545	
Multilayer insulation	<u>909</u>	
Sub-total	145,651	
Helium - 30,000 liters @ 0.126 kg/P	3,773	
Magnets	170,455	
Magnet attachment structure and auxiliaries	<u>47,727</u>	
Total Supported Weight	367,606	kg

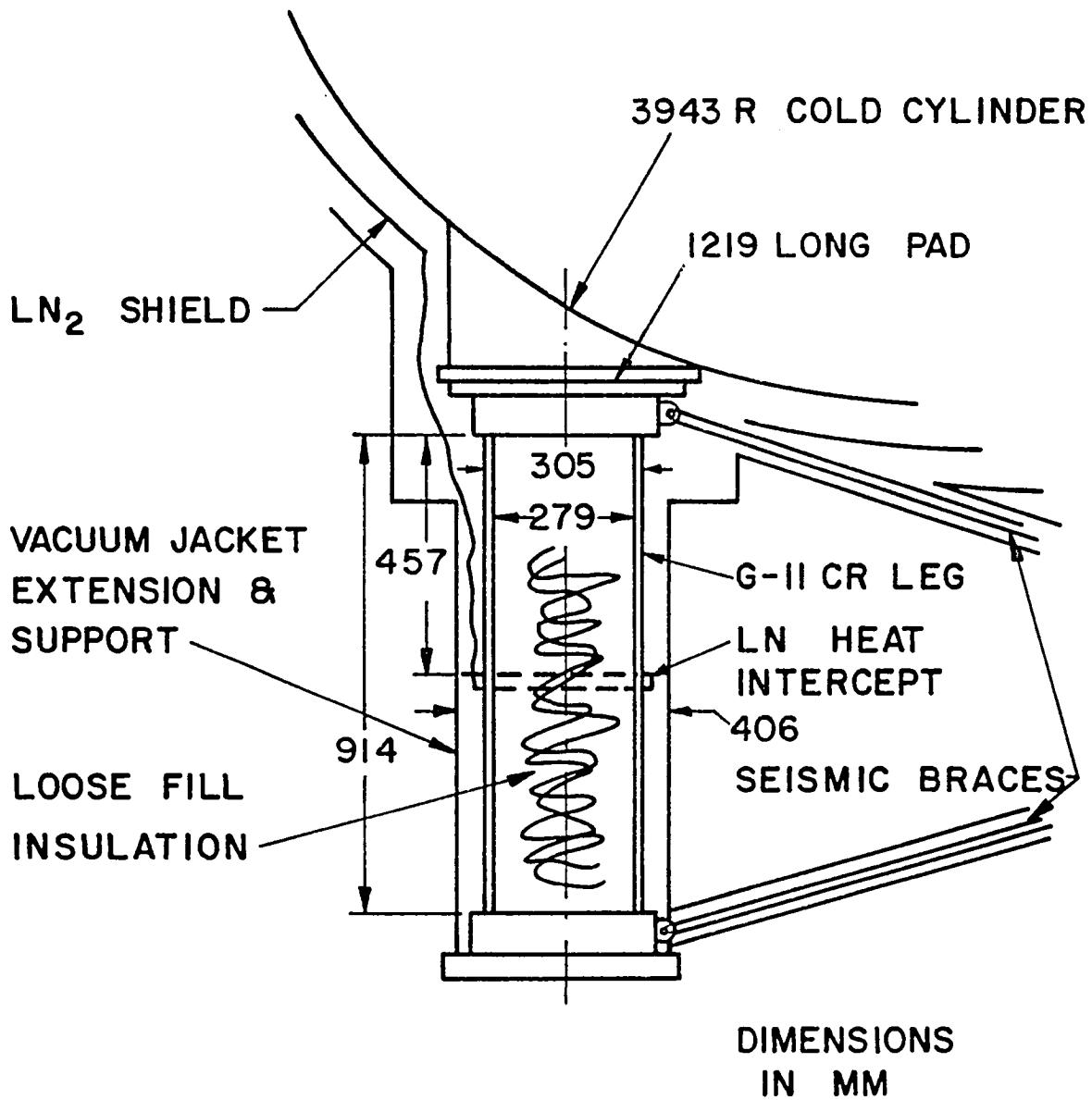


FIGURE V.8
LEG ASSEMBLY CONCEPT

V.8 Cryostat Heat Leak

Static heat leak of the cryostat is given in Table V-4. Most of the heat leak is due to solid conduction and is accurate to about 15%. The performance of multilayer insulation is reflected in the end bell and outer cylinder heat leaks. Quality of the installation of insulation can affect these heat leaks - 10 to + 50%. To realize the calculated heat leak of the egg crate assembly it is important to get the insulation spaces well filled with Perlite. This can be done with an industrial vacuum cleaner and appropriate end filters plus a shaker or vibrator to compact the powder.

TABLE V-4
STATIC HEAT LEAK AND CRYOGEN CONSUMPTION

Item	Helium		Nitrogen	
	Q	L/h	Q	L/h
Legs and Braces	2.36 W		16.73 W	
Egg Crate	24.52		416.87	
End Bells	1.7		30.47	
Outer Cylinder	6.19		103.14	
Stacks	6.61		24.5	
Contingency	<u>3.62</u>		<u>32.79</u>	
Totals	45.0 W	*63.5 L/h	600.0 W	14 L/h

*0.7089 W (heat leak into helium) \cong 1 liter/h evaporated

VI. CRYOGENIC SYSTEM

VI.1 INTRODUCTION

A schematic of the proposed cryogenic system is shown in Fig. VI.1 which is an enclosed drawing. Major elements of the system include the magnet cryostat, helium liquefier, helium storage dewar, helium recovery compressor, 18 atm. helium gas storage, and a cooldown loop. Design of the system is based on the following criteria:

- Reasonable cool down time of eight to ten days.
- Adequate liquid storage to fill the magnet cryostat with reserve to meet daily or five-day week operating deficits.
- Available liquid storage capacity sufficient to empty the cryostat without loss of helium.
- Liquefaction capacity to maintain scheduled operations on either a continuous or five-day week basis.
- Sufficient compressor capacity to handle the maximum planned rate of gas evolution without helium loss.
- Helium gas storage for all of the helium in the system to permit an indefinite shut down.

Considerations relating to the design and operation of each part of the system are discussed in the following paragraphs.

VI.2 MAGNET POWER LEADS

There are twenty-four 11,000 A leads for the 14 magnets, not 28 leads, since the two R coils on each side are series connected. Full load losses for

standard commercial gas cooled leads are 1.4×10^{-3} liters per hour of helium per ampere for one lead and 40% less or 0.84×10^{-3} liter per hour per A rating at zero current. For the twenty-four 11 kA leads these helium loss rates are 370 and 222 liters/hour respectively. However, since cold return gas is not otherwise utilized, the leads are cooled with the excess gas with significant reductions in lead losses. As an example, the optimum L/A ratio can be exceeded to markedly reduce zero current static losses, which is most important for the expected long standby periods at 4.2 K with $I = 0$ in all magnets.

The proposed design incorporates all of the above features. Since there is excess helium gas at both 1/4 load and full load, the leads will be run at 0.08 g/s/1000 A instead of the optimum 0.046 g/s/1000 A. Flow controllers will be installed on each lead for this purpose. The leads are about 1524 mm instead of the typical 762 mm long to reduce the no load losses at the expense of somewhat higher full current losses. Although the design is not considered optimized the improved performance is listed in Table VI-1.

TABLE VI-1
PREDICTED LEAD LOSSES

<u>Mode</u>	<u>Heat Input - W</u>	<u>Helium Loss - L/h</u>
Zero Current	78.6	110.9
1/4 Load	81.2	114.5
Full Load	120	169.3

VI.3 OPERATING LOSSES

AC losses for the system for 1/4 and full load conditions from Tables IV-11 and 12 are combined with the static heat leak, lead losses, and conductor joint losses to compile total heat loads in Table VI-2. These losses determine the size of the liquefaction and refrigeration system.

VI.4 COMPONENT DESIGN AND SIZING

The MSBS system may be operated either continuously or on a five-day week basis with weekends for reliquefying helium. As shown below, the two operating plans influence the size of individual components but the total plant cost is about the same for either. In both cases the 30,000 liter cryostat is assumed to have been cooled down to 20 K after which 4000 liters of liquid helium is provided for final cooldown.

The liquefier is sized first based on continuous operation with daily liquid consumption as follows.

Full Load	3120 L/h x 2	=	6,240 L
One-quarter Load	590 L/h x 8	=	4,720 L
Zero Load	175 L/h x 14	=	<u>2,450 L</u>
Total			13,410 L/day
Liquefier Size	= 13,410/24 h	=	560 L/h

The liquid helium storage dewar is sized by the liquid deficit from full load (2 h) and quarter load (8 h) which must be made up during zero load (14 h).

TABLE VI-2
MAGNET CRYOSTAT OPERATING LOSSES

<u>Loss</u>	<u>Zero Load</u>	<u>1/4 Load</u>	<u>Full Load</u>
Conductor (AC)	--	187.78	379.4
S.S. Strip (AC)	--	1.58	25.44
Structural Eddy Current	--	97.52	1560
Conductor Joints	--	5.13	82
Leads	78.6	81.2	120
Static Heat Leak	<u>45</u>	<u>45</u>	<u>45</u>
Total Losses - W	123.6 W	418.21 W	2211.84 W
Helium Consumption - L/h	175	590	3120

It is not considered feasible to oversize the liquefier to match the full load of 3120 L/h since the average load is only 560 L/h. The total deficit per day is:

$$\text{Liquid Deficit} \quad 2(3120 - 560) \quad = \quad 5120 \text{ L}$$

2 h - full load

$$\text{Liquid Deficit} \quad 8(590 - 560) \quad = \quad 240$$

8 h - quarter load

$$\text{Total Deficit per Day} \quad = \quad 5360 \text{ L}$$

The recovery compressor is sized by the maximum helium off-gas rate during full load when 3120 L/h of liquid helium evaporates of which 560 L/h is reliquefied and 2560 L/h is compressed into 18 atm storage. The 2560 L/h is converted into 1 atm, 21.1 C gas at the rate of 0.7576 m³/L or

$$V_{\text{gas}} = 2560 \times 0.7576 = 1939.4 \text{ m}^3/\text{h}$$

and the recovery compressor size is

$$V/60 = 32.58 \text{ m}^3/\text{min} \text{ (1150 cfm)}.$$

The storage dewar size is:

Final cryostat cooldown	4,000 liters
Fill cryostat	30,000
Daily running deficit	<u>5,360</u>
	39,360
Contingency	<u>8,140</u>
Dewar size	47,500 liters

The gas amount is taken as 10% more gas than from the liquid in the storage dewar,

$$V_{\text{gas}} = (47,500) (1.1) (0.7576) = 39,644 \text{ m}^3 ,$$

which at 18 atm requires a gas storage size of

$$V_{18} = 2,226.3 \text{ m}^3 .$$

Table VI-3 is a component summary.

TABLE VI-3
CRYOGENIC COMPONENTS FOR CONTINUOUS OPERATION

Liquefier	560	L/h
Recovery Compressor	32.58	m ³ /min (1150 cfm)
Storage Dewar	47,500	L
Gas (at 1 atm, 21.1 C)	39,644	m ³
Gas Storage at 18 atm	2,226.3	m ³

By the same analysis the components for a five-day week are listed below. In comparison, the liquefier is smaller and the recovery compressor, storage dewar and gas storage are larger. For a five-day week the component sizes are given in Table VI-4.

TABLE VI-4
CRYOGENIC COMPONENTS FOR FIVE-DAY WEEK OPERATION

Liquefier	450 L/h*
Recovery Compressor	34 m ³ /min (1200 cfm)
Storage Dewar	56,000 L
Gas (at 1 atm, 21.1 C)	46,723 m ³
18 atm Storage	2,624 m ³

* Liquefiers would be slightly oversized to make up for dewar losses which should fall in the range of 0.15 to 0.2% per day or approximately 4 L/h.

VI.5 COMPONENT DISCUSSION

Liquefier: While not an off-the-shelf item, either the 560 or 450 L/h liquefier is well within the state-of-the-art and smaller than several which have been in commercial service for 10 to 15 years. There will be multiple bidders for this item.

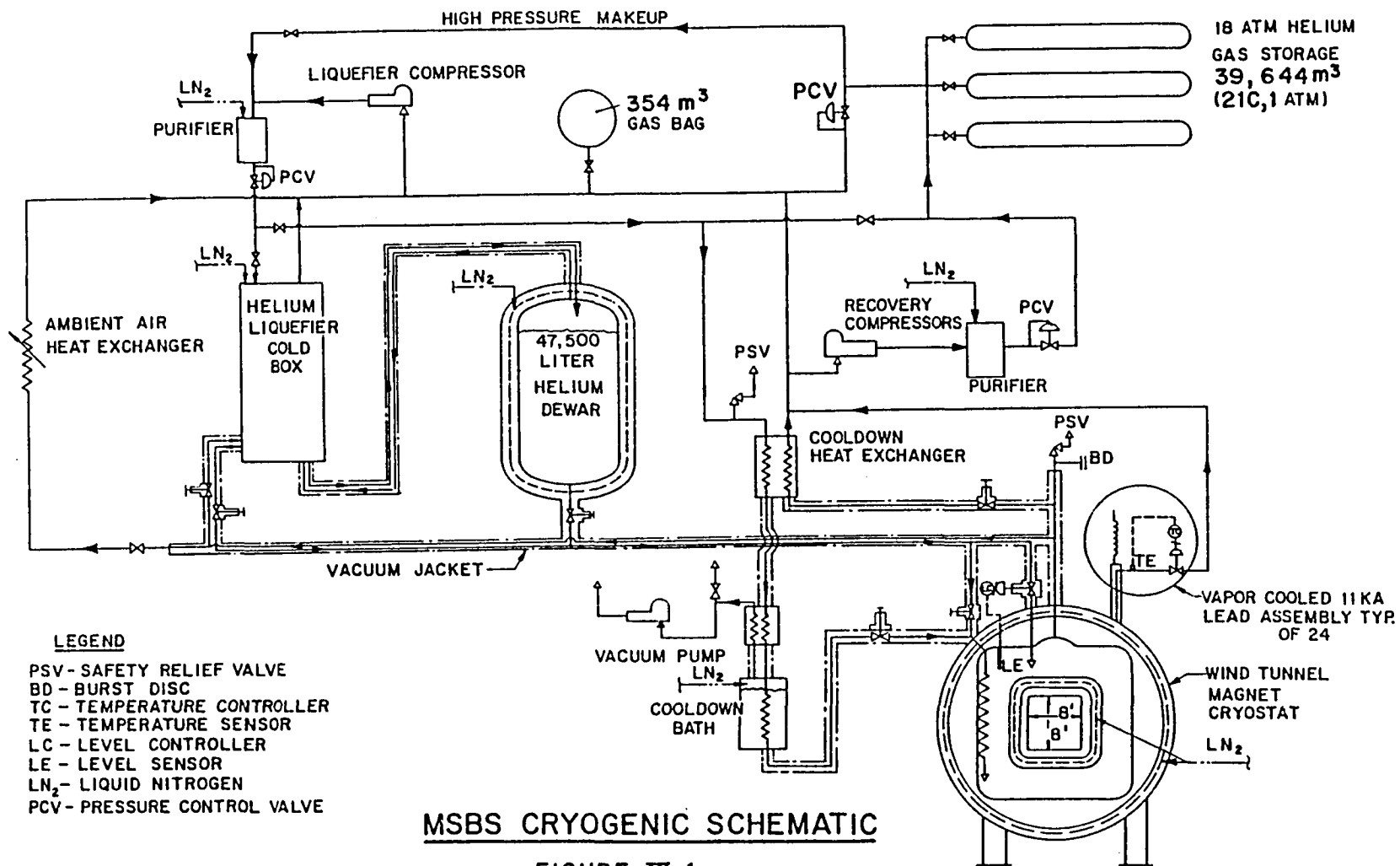
Dewar: The design anticipates a multilayer insulated dewar incorporating a liquid nitrogen cooled shield. A similar 19,000 liter helium vessel designed by one of the investigators has a measured loss rate of 0.13% per day

and it is reasonable to expect 0.1% for a larger dewar. However, such dewars are considered difficult to build and there will be fewer bidders than on the liquefier. It should be noted that the proposed installation of the dewar is about 10.7 m above the cryostat so that it can be maintained at low pressure with liquid supplied by gravity flow.

Gas Handling: The gas handling system consists of the recovery compressor, gas bag, and 18 atm storage. The compressor will be a four-stage oil lubricated machine equipped with oil removal components and a small cryogenic purifier so that only high purity helium is stored. The commercially available 354 m³ gas bag provides a low pressure buffer volume for both the liquefier and recovery compressor. As described above, 18 atm storage is sized to hold all of the helium in the system for indefinite shutdown.

Preliminary plans were to utilize a high pressure recovery compressor and store helium at 150 atm. However, storing at 18 atm utilizes commercial propane tanks which are much cheaper than high pressure cylinders. The main disadvantage of lower pressure storage is that the 20 tanks required, each 2.74 m in diameter and 20.12 m long, take considerably more space than high pressure storage cylinders. One advantage of low pressure storage, besides cost, is that it matches the liquefier operating pressure so that the recovery and liquefier compressors can be used interchangeably.

Cooldown System: Only helium will be used to cool down the cryostat to avoid the possibility of contamination and the difficulty of removing nitrogen if it is introduced. As shown in the MSBS Cryogenic Schematic, Fig. VI.1, the system is set up so that both liquefier and recovery compressors work in



parallel for this function. For the 560 L/h liquefier, flow is about $49.55 + 32.58 = 82.13 \text{ m}^3/\text{min}$. For the 450 L/h liquefier the available flow is approximately $39.64 + 33.98 = 73.62 \text{ m}^3/\text{min}$. In either case, flow goes through a special cooldown heat exchanger to a liquid nitrogen bath and on to the cryostat. At the start, the level in the bath will be controlled so that entering cold gas will not be more than 100 K colder than the cryostat. As the cooldown proceeds the bath will be filled so that 78 K gas will be available. Since it is important to get all possible cooling from liquid nitrogen, the LN₂ system will be equipped with a blower-type vacuum pump to reduce the bath temperature to 65 K.

When the cryostat has been cooled to approximately 70 K, use of the cooldown system will be discontinued and the liquefier will be used as a cold gas refrigerator. This mode of operation will be continued until the temperature is about 20 K. At 20 K the specific heat of the magnets and cryostat is low enough that cooldown can be completed with about 4000 liters of liquid helium. Thus, when the cryostat reaches 20 K the liquefier will switch back to the storage dewar and liquid will be withdrawn from the storage dewar to finish the cooldown and fill the cryostat in one continuous operation.

Liquid and Cold Gas Transfer Lines: Necessary vacuum jacketed lines are indicated on the flow schematic. Of these, the principal line runs from the dewar to the cryostat, with branches to the two Drag coils, with a cold gas extension beyond the dewar to the liquefier cold box. A sketch of this coaxial line is shown in Fig. VI.2. In liquid service this line will function as follows:

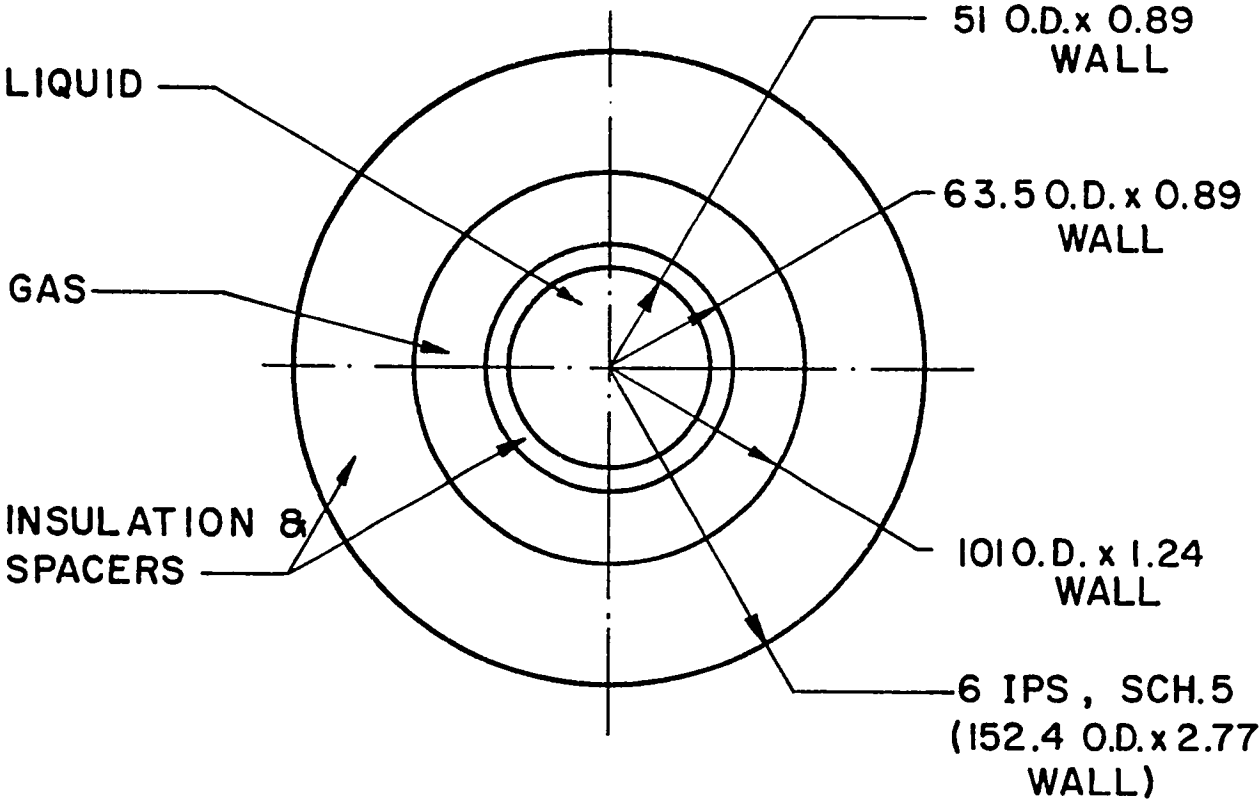


FIGURE VI. 2

CO - AXIAL TRANSFER LINE

DIMENSIONS IN MM

- Liquid flows in the inner line at 0.07 to 0.136 atm above the cryostat pressure making the liquid 0.1 to 0.15 K warmer than liquid and gas in the cryostat.
- Liquid is throttled to cryostat pressure as it is delivered with a reduction in temperature and a small percentage of gas flashing to vapor.
- The slightly colder vapor returns in the gas annulus. This cold gas intercepts heat and essentially creates a zero heat leak environment for the liquid line. The purpose of the insulation space between the lines is to prevent the two passages from forming a heat exchanger whenever the gas return is warmer as in the cooldown operation.

Controls and Safety Devices: At this stage only rudimentary attention has been devoted to controls necessary for functioning of the cryogenic system. As shown on the schematic, the cryostat will be equipped with a level indicator and controller for the main volume and each Drag coil reservoir and all three will be protected by relief valves and burst discs. Each lead will have a flow controller and consideration will be given to an overall monitor and control system to ensure that flows are properly distributed at times of less than full flow. The compressors will be equipped with bypass circuits and standard over and under pressure switches for automatic unattended operation.

VI.6 Component Cost Estimates

Cost comparisons between the continuous seven-day system and the five-day system are listed in Table VI-5. The system costs are almost identical and

TABLE VI.5
CRYOGENIC SYSTEM COST ESTIMATES

<u>Continuous Seven-Day Operation</u>	
560 Liter Liquefier	\$1,977,000
Dewar	509,000
Recovery Compressor	328,000
Gas Storage	<u>550,000</u>
Sub-Total	3,364,000
Cooldown System	150,000
VJ Pipe and Valves	100,000
Balance of Plant*	<u>150,000</u>
Total	\$3,764,000

<u>Five-Day Operation</u>	
450 Liter Liquefier	\$1,700,000
Dewar	572,000
Recovery Compressor	343,000
Gas Storage	<u>633,000</u>
Sub-Total	3,248,000
Cooldown System	150,000
Vacuum Jacketed Pipes and Valves	100,000
Balance of Plant*	<u>150,000</u>
Total	\$3,648,000

*No buildings or civil work.

lead to the choice of the continuous system as being less restrictive, although five-day/week operation is probably adequate and \$116,000 less expensive.

VI.7 COOLDOWN ANALYSIS:

Cooldown calculations are based on the 560 L/h liquefier (seven-day week) and 32.58 m³/min recovery compressor for a total helium flow of 82.13 m³/min. Also, maximum temperature difference is limited to 100 K. Below 70 K only the liquefier compressor is used and liquid helium is used directly for final cooling from 20 to 4.2 K. The estimated cooldown time is:

300 - 70 K	132 hours
70 - 20	44
20 - 4.2	<u>4</u>
Total	180 hours, 7 1/2 days.

VI.8 OPERATING PLAN

The summary operating plan for the cryogenic system from a completely warm start might consist of the following steps:

1. Purge and fill the entire system with helium gas.
2. Start the liquefier and fill the storage dewar. Including dewar cooldown, this will take about 96 hours for the seven-day system and 136 hours for the five-day system.
3. Cooldown and fill the magnet cryostat. Allow eight days total for this step.

4. Operate the cryostat as scheduled
 - a. Whenever gas flow exceeds the liquefier capacity the recovery compressor will cycle on to pump gas back to 18 atm storage.
 - b. To the extent possible the liquefier will run continuously when there is liquid helium in the cryostat.
5. At the end of an operating program with the wind tunnel, or at any time the system is to be down more than two weeks, liquid should be transferred back to the dewar and the cryostat allowed to warm up to 78 K by continuing to supply LN₂ to the shields. Restart can then be accomplished in three to four days.
6. Since the storage dewar will only lose 2,500 to 3,000 liters per month, it should be left cold except for very long shut downs of three months or more. When the dewar is idling, gas is collected in the gas bag and can be pumped back to 18 atm storage every three or four days.
7. For long term shut down, liquid may be sent through the ambient vaporizer at a rate consistent with the recovery compressor capacity and pumped to the gas storage facility.

VII. SCALING RELATIONS

Scaling relations are developed between a L ft x L ft wind tunnel and the present reference 8 ft x 8 ft tunnel as to force, torques and currents.

VII.1 FORCE AND TORQUE SCALING

All forces F_x , F_y , or F_z are related to the square of the model length which is linearly related to the tunnel length L. Thus the required static forces for an L' x L' tunnel are those listed in Table II-1 multiplied by the square of L/8.

$$F_L/F_8 = (L/8)^2$$

The new torque requirements are therefore given by

$$T_L/T_8 = (L/8)^3$$

VII.2 MODEL CORE SCALING

If magnetized iron or permanent magnets are used for either the model core or the wing then the pole strength for an L' x L' tunnel will be increased by the square of L/8. Therefore the new pole strengths and magnetic moments are

$$Q_L/Q_8 = (L/8)^2$$

and $M_L/M_8 = (L/8)^3$.

Accordingly to produce the required forces or torques the magnetic field values at the tip of the wing or on the model core remain the same and the field gradients will be scaled as

$$\nabla B_L / \nabla B_8 = 8/L \quad .$$

If a superconducting coil is the core model then scaling toward greater length will be more favorable since the new pole strength is related to the 8' x 8' tunnel by more than the square of the L/8, as seen in Table III-1. For a 6.1 tesla coil at 3×10^8 A/m³ current density, the relation is

$$Q_L / Q_8 = 2.5 \times 10^4 \{ (R_L - \delta)^3 - (R_L - \delta - 1.61 \times 10^{-3})^3 \}$$

where $R_L = 0.0635 (L/8)$

and $\delta = 0.006 \quad .$

The model coil length will be scaled as $\{(\lambda - 5)/70\}$ where

$$\lambda = 75 L/8 \quad .$$

To produce the required forces and torques, the magnetic field values at the tip of the superconducting core coil are scaled as

$$\frac{B_L}{B_8} = \frac{Q_8}{Q_L} \times \frac{70}{\lambda - 5} \times \left(\frac{L}{8}\right)^3 = \xi$$

Table VII-1 is a list of B_L/B_8 and $\nabla B_L/\nabla B_8$ for model cores of soft magnetic material and for model cores of a superconducting coil as a function of L/8.

TABLE VII-1

SCALING OF MAGNETIC FIELD AND FIELD GRADIENT AT THE
 MODEL FOR SUPERCONDUCTING COIL CORES AND MAGNETIC
 CORES AS A FUNCTION OF L/8

L/8	SUPERCONDUCTING COIL		MAGNETIC MATERIAL	
	$\xi = B_L/B_8$	$\nabla B_L/\nabla B_8$	B_L/B_8	$\nabla B_L/\nabla B_8$
0.5	1.65	3.3	1.0	2.0
0.6	1.55	3.59	1.0	1.667
0.8	1.22	1.52	1.0	1.25
1.0	1.0	1.0	1.0	1.0
1.6	0.798	0.499	1.0	0.625
2.0	0.744	0.372	1.0	0.5

VII.3 AMPERE METER SCALING

The total ampere meters, IS, may be divided into two parts. The first part, IS₁, is related to the x, y, z forces, and the pitch and yaw torques. The second part, IS₂, is related to the roll torque requirement plus the cross coupling on the Z and Y coils due to the roll coils. Table VII-2 summarizes the ampere meter requirement for the 8' x 8' tunnel.

TABLE VII. 2
AMPERE METER REQUIREMENT FOR THE 8' x 8' WIND TUNNEL

	Drag Coils	Z Coils	Y Coils	Roll Coils	Total IS
IS ₁ (MAm)	309	73	16	--	398
IS ₂ (MAm)	53	13	84	207	357

For any L' x L' tunnel the total ampere meters IS is

$$IS = IS_1 (L/8)^2 \xi + IS_2 (L/8)^2 ,$$

where $\xi \equiv B_L/B_8$.

Ampere meters (IS) and ampere turns (NI) are listed in Table VII-3 as a function of L/8.

TABLE VII-3
TOTAL AMPERE METERS AS A FUNCTION OF L/8

L/8	NI_L/NI_8	IS_L/IS_8	IS (MAm)
0.5	0.670	0.335	253
0.6	0.788	0.473	357
0.8	0.894	0.715	540
1.0	1.000	1.000	755
1.6	1.43	2.281	1722
2.0	1.724	3.449	2604

VIII. COST ESTIMATE

The cost estimate is \$29,939,000 for Case 1 - Alternate G. Costs are estimated for the completed project consisting of preliminary design, final design, construction, installation, and test. The cost of items not addressed in this study are transcribed directly from NASA CR 165917 for Case 1 - Alternate G. Such items are marked by an asterisk * in the following chart. Other items have been scaled when there is simple cost dependence on size, weight, stored energy and there is no apparent reason to change the cost basis. Particularly retained are those costs which include industrial management and industrial accounting.

The independent costs presented here cover the magnet system, the structure, the cryogenic system and the power supplies. Even though this is a different design it is possible to show that independently costed items are consistent with the NASA CR 165917 cost basis. The differences are due to reduction in materials and simplicity of design with the same industrial based cost rates.

The cost estimate is for a system which meets the roll torque requirement, uses stainless steel dewars and structure even with the eddy current loss penalty, has adequate sized Y coils, and accounts for maximum cross coupling disadvantages. There is no magnetization coil. There is no factory test 1.3.14 since the dewar is constructed in place. The installation cost 1.3.16 is listed separately but is complementary to support structure manufacturing 1.3.12 where a full 10 \$/lb is allowed for structure. The full value of 1.3.2 is transcribed from NASA CR 165917 even though machines and

tooling for steel construction are more routine than for large epoxy coil structures. Position sensors and controls are not addressed in this study and such costs are transcribed from NASA CR 165917. The cryogenic system includes a recovery compressor and cooldown system.

TABLE VIII-1

MSBS COST ESTIMATE (CASE 1 - ALTERNATE G) - CONTROL BASED ON
 0.1% I_{\max} AT 10 Hz IN ALL COILS SIMULTANEOUSLY
 COSTS IN THOUSANDS \$

1.0	MSBS		29,939
1.1	PRELIMINARY DESIGN PHASE		919
1.1.1	SYSTEM ENGINEERING	*	120
1.1.2	MAGNET SUBSYSTEMS PRELIMINARY DESIGN		151
1.1.3	CRYOGENICS SUBSYSTEMS PRELIMINARY DESIGN		60
1.1.4	POWER SUPPLY AND PROTECTION PRELIMINARY DESIGN		30
1.1.5	POSITION SENSORS SUBSYSTEMS PRELIMINARY DESIGN	*	131
1.1.6	CONTROL SUBSYSTEMS PRELIMINARY DESIGN	*	87
1.1.7	SUPPORT STRUCTURES PRELIMINARY DESIGN		138
1.1.8	MANUFACTURING ENGINEERING		30
1.1.9	VERIFICATION TESTING	*	40
1.1.10	PRELIMINARY DESIGN PHASE PROGRAM MANAGEMENT	*	132
1.2	FINAL DESIGN PHASE		2,853
1.2.1	SYSTEM ENGINEERING		178
1.2.2.	MAGNET SUBSYSTEMS FINAL DESIGN		306
1.2.3	CRYOGENICS SUBSYSTEMS FINAL DESIGN		300
1.2.4	POWER SUPPLY AND PROTECTION FINAL DESIGN	*	95
1.2.5	POSITION SENSORS SUBSYSTEMS FINAL DESIGN	*	419
1.2.6	CONTROL SUBSYSTEMS FINAL DESIGN	*	350
1.2.7	SUPPORT STRUCTURES FINAL DESIGN		492

1.2.8	MANUFACTURING ENGINEERING		178
1.2.9	VERIFICATION TESTING	*	144
1.2.10	FINAL DESIGN PHASE PROGRAM MANAGEMENT	*	391
1.3	MANUFACTURING INSTALLATION, CHECKOUT PHASE		26,167
1.3.1	ENGINEERING SUPPORT OF MANUFACTURING, INSTALLATION, CHECKOUT		683
1.3.2	MACHINES AND TOOLING	*	1,458
1.3.3	Z GRADIENT COILS MANUFACTURING		505
1.3.4	Y GRADIENT COILS MANUFACTURING		551
1.3.5	ROLL COILS MANUFACTURING		1,146
1.3.6	DRAG COILS MANUFACTURING		2,182
1.3.7	MODEL CORE COIL MANUFACTURING		350
1.3.8	CRYOGENICS SUBSYSTEMS MANUFACTURING		3,764
1.3.9	POWER SUPPLY AND PROTECTION MANUFACTURING		6,318
1.3.10	POSITION SENSORS SUBSYSTEMS MANUFACTURING	*	1,068
1.3.11	CONTROL SUBSYSTEMS MANUFACTURING	*	1,046
1.3.12	SUPPORT STRUCTURE MANUFACTURING		2,813
1.3.13	VERIFICATION TESTING		144
1.3.14	FINAL FACTORY INSPECTION AND TEST		--
1.3.15	BOX, PACK AND SHIP		310
1.3.16	INSTALLATION OF MSBS		1,000
1.3.17	CHECKOUT AND ACCEPTANCE TESTING	*	1,012
1.3.18	MANUFACTURING, INSTALLATION, CHECKOUT PHASE PROGRAM MANAGEMENT	*	1,817

*Directly from NASA CR 165917.

IX. CONCLUSION

The MSBS design presented satisfies all specified requirements with consideration given to most major design problems. Each coil is optimized as to location and shape. Stainless steel structure is used throughout. Structural eddy current losses are large but tolerable. The cryogenic system is sized primarily by the structural eddy current losses which arise during the two hour full load period of maximum continuous AC losses at 10 Hz.

Two unique features of the design are the compact model core superconducting solenoid and the compact magnet design with race track roll coils. Considerable design simplicity and reduced heat leak results from mounting all magnets in one pool cooling dewar with internal cold structure and eliminating heavy cold steel structure between coils and the model.

The cost estimate is about \$30,000,000 for the MSBS for an 8 x 8 ft tunnel operating at 0.9 Mach.

X. RECOMMENDATIONS FOR FUTURE STUDIES

The present study demonstrates technical feasibility of the MSBS and provides cost estimates which seem economically feasible. The general design is simple and straightforward, and should be accepted with confidence.

Four basic key items of the MMI design are:

1. Model core superconducting magnet and cryostat
2. Permanent magnet wing assembly
3. Helium leak-tight electrical breaks
4. Structural insulated segmentation.

The major recommendation is to implement a program aimed at verifying and improving these four basic key items.

The second recommendation for future studies is to continue to study this design aiming towards three general goals.

- To simplify and improve the structural design for optimum usage
- To explore cost-benefit compromises for such major options as superfluid cooling, supercritical cooling, control frequency limits other than 10 Hz, and wind tunnel sizes other than 8 ft x 8 ft.
- To prepare and evaluate several advanced conceptual designs embodying the best features of the above work.

1. Report No. NASA CR-3802		2. Government Accession No.		3. Recipient's Catalog No.	
4. Title and Subtitle MAGNETIC SUSPENSION AND BALANCE SYSTEM STUDY				5. Report Date July 1984	
				6. Performing Organization Code	
7. Author(s) R. W. Boom, Y. M. Eyssa, G. E. McIntosh, and M. K. Abdelsalam				8. Performing Organization Report No.	
				10. Work Unit No.	
9. Performing Organization Name and Address Madison Magnetics, Inc. 216 Walnut Street Madison, Wisconsin 53705				11. Contract or Grant No. NAS1-17428	
				13. Type of Report and Period Covered Contractor Report 6-83 to 3-84	
12. Sponsoring Agency Name and Address National Aeronautics and Space Administration Washington, D.C. 20546				14. Sponsoring Agency Code 505-31-53-10	
15. Supplementary Notes Langley Technical Monitor: Richmond P. Boyden Final Report					
16. Abstract <p>A compact design for a superconducting magnetic suspension and balance system is developed for a 8 ft. x 8 ft. transonic wind tunnel. The main features of the design are: a compact superconducting solenoid in the suspended airplane model; permanent magnet wings; one common liquid helium dewar for all superconducting coils; effecient new race track coils for roll torques; use of established 11 kA cryostable AC conductor; acceptable AC losses during 10 HZ control even with all steel structure; and a 560 liter/hour helium liquefier. Considerable design simplicity, reduced magnet weights, and reduced heat leak results from using one common dewar which eliminates most heavy steel structure between coils and the suspended model. Operational availability is thought to approach 100% for such magnet systems. The weight and cost of the magnet system is approximately one-third that of previous less compact designs.</p>					
17. Key Words (Suggested by Author(s)) Magnetic suspension Magnetic balance Superconducting magnets Wind tunnel balance			18. Distribution Statement Unclassified - Unlimited Subject Category 09		
19. Security Classif. (of this report) Unclassified		20. Security Classif. (of this page) Unclassified		21. No. of Pages 117	22. Price A06



National Aeronautics and
Space Administration

Washington, D.C.
20546

Official Business

Penalty for Private Use, \$300

THIRD-CLASS BULK RATE

Postage and Fees Paid
National Aeronautics and
Space Administration
NASA-451



NASA

POSTMASTER: If Undeliverable (Section 158
Postal Manual) Do Not Return
